TECHNICAL MEMORANDUM
X-208

HEAT TRANSFER TO 36.75° AND 45° SWEPT BLUNT LEADING

EDGES IN FREE FLIGHT AT MACH NUMBERS FROM

1.70 TO 2.99 AND FROM 2.50 TO 4.05

By Robert L. O'Neal

Langley Research Center
Langley Field, Va.

Declassified April 23, 1962

NATIONAL AERONAUTICS AND SPACE ADMINISTRATION

WASHINGTON   March 1960

NATIONAL AERONAUTICS AND SPACE ADMINISTRATION

TECHNICAL MEMORANDUM X-208

HEAT TRANSFER TO 36.75° AND 45° SWEPT BLUNT LEADING

EDGES IN FREE FLIGHT AT MACH NUMBERS FROM

1.70 TO 2.99 AND FROM 2.50 TO 4.05*

By Robert L. O'Neal

SUMMARY

A flight investigation has been conducted to study the heat trans-
fer to swept-wing leading edges. A rocket-powered model was used for
the investigation and provided data for Mach number ranges of 1.78 to
2.99 and 2.50 to 4.05 with corresponding free-stream Reynolds number per
foot ranges of 13.32×10^6 to 19.90×10^6 and 2.85×10^6 to 4.55×10^6.
The leading edges employed were cylindrically blunted wedges, three of
which were swept 45° with leading-edge diameters of 1/4, 1/2, and 3/4 inch
and one swept 36.75° with a leading-edge diameter of 1/2 inch. In the
high Reynolds number range, measured values of heat transfer were found
to be much higher than those predicted by laminar theory and at the larger
values of leading-edge diameter were approaching the values predicted by
turbulent theory. For the low Reynolds number range a comparison between
measured and theoretical heat transfer showed that increasing the leading-
edge diameter resulted in turbulent flow on the cylindrical portion of
the leading edge.

INTRODUCTION

Current interest in high-speed aircraft has necessitated that a
considerable amount of research be devoted to the problem of aerodynamic
heating of wing leading edges. References 1 to 8 have indicated that
the two principal leading-edge geometry variations for reducing the heat
transfer are sweeping and blunting the leading edge.

It was shown in reference 4 that at low Reynolds numbers the decrease
in heat transfer associated with increased leading-edge sweep can be pre-
dicted by theory for a laminar boundary layer. In references 6 to 8 it

---

*Title, Unclassified.

is shown that at high Reynolds numbers it is possible for sweepback to induce turbulent flow on a leading edge, apparently caused by the instability of the three-dimensional boundary layer, and result in heat transfer equal to or greater than that which would exist for laminar-flow no-sweep conditions. A theory is presented in reference 6 for predicting the average heat transfer around a swept leading edge in a turbulent environment. Recent work by Beckwith and Gallagher (ref. 7) presents a theory for predicting local values of leading-edge heat transfer for larger sweep angles in the presence of a turbulent boundary layer.

It was shown theoretically and experimentally in reference 4 that for a laminar boundary layer an increase in leading-edge bluntness results in a decrease in heat transfer. This was also found to be true for the turbulent case in reference 7. As part of the effort to provide a better understanding of the effects of leading-edge geometry on aerodynamic heating of leading edges at high Mach numbers and Reynolds numbers, a free-flight investigation was conducted at the NASA Wallops Station to measure the heat transfer to swept leading edges of various degrees of bluntness. The leading-edge segments utilized in this investigation were cylindrically blunted wedges, three of which were swept 45° with leading-edge diameters of $1/4$, $1/2$, and $3/4$ inch, and one swept 36.75° with a leading-edge diameter of $1/2$ inch. This investigation covered Mach number ranges of 1.78 to 2.99 and 2.50 to 4.05 with corresponding free-stream Reynolds number per foot ranges of 13.32×10^6 to 19.90×10^6 and 2.85×10^6 to 4.55×10^6.

SYMBOLS

b	spanwise distance, in.
C_p	pressure coefficient, $\dfrac{p_l - p_\infty}{0.7 p_\infty M^2}$
c	distance along chord, parallel to free stream, in.
c_p	specific heat of air at constant pressure, Btu/lb-$^\circ$F
c_w	specific heat of wall material at T_w, Btu/lb-$^\circ$F
D	leading-edge diameter
g	gravitational constant, 32.2 ft/sec^2
h	local aerodynamic heat-transfer coefficient, Btu/sq ft-sec-$^\circ$F

M	Mach number
N_{St}	Stanton number, $h/gc_p\rho_\infty V_\infty$
p	pressure, lb/sq ft
N_{Pr}	Prandtl number
q	heating rate, Btu/sq ft-sec
R	Reynolds number based on 1 foot and free-stream conditions
R_D	Reynolds number based on leading-edge diameter and free-stream conditions
S	distance measured along segment wall perpendicular to leading edge, ft
T	temperature
T_w	average temperature across wall
t	time, sec
V	velocity, ft/sec
Λ	leading-edge sweep angle, deg
Φ	azimuth angle measured from forward stagnation point perpendicular to leading edge, deg (see fig. 3)
ρ	density of air, slugs/cu ft
ρ_w	density of wall material, lb/cu ft
τ	thickness of wall, ft

Subscripts:

aw	adiabatic wall
l	local conditions just outside boundary layer
s	outside surface of wall

t   stagnation conditions

∞   undisturbed free stream ahead of model

MODEL, INSTRUMENTATION, AND TEST

The vehicle used in this investigation was a body of revolution consisting of an ogive-cylinder-flare configuration. Four wing leading-edge segments were symmetrically mounted 90° apart at 0° incidence on the cylindrical portion of the vehicle as shown by the sketch of figure 1 and the photograph of figure 2.

The leading-edge segments were made of Inconel with cylindrical leading edges faired tangent to flat surfaces inclined 4.27° from the chord plane as shown in figure 3. Each of the segments had a span of 4 inches measured from the cylindrical wall of the model. Three of the leading-edge segments were swept 45° with leading-edge diameters of 1/4, 1/2, and 3/4 inch and the fourth segment was swept 36.75° with a leading-edge diameter of 1/2 inch. The outside surface of each segment was polished to a roughness of 5 microinches measured by a comparative microscope.

Each segment was instrumented with chromel-alumel thermocouples spotwelded to the inside surface at the locations indicated in figure 3. The skin thickness at each thermocouple location was measured and was found to be 0.049 inch. Resin filler blocks were used to close off the trailing edge and tip of each segment to protect the interior from the airstream. A local pressure was measured or the flat portion of the 45° swept, 3/4-inch-diameter segment at the location indicated in figure 3.

The flight vehicle was instrumented with an NACA eight-channel telemeter which transmitted temperature, pressure, and acceleration data. Details of the thermocouple telemetering technique can be found in reference 9.

A CW Doppler radar unit was used to measure model velocity and an NACA modified SCR-584 radar unit provided data for obtaining the position of the model in space. Atmospheric data and wind velocity were obtained by means of a radiosonde launched shortly before the time of model launching and tracked by a Rawin set, AN/GMI-1A.

The test vehicle and boosters are shown in firing position in figure 4. The propulsion system consisted of three stages of rocket motors. The first stage was an M5 JATO rocket motor and the second and third

stages were JATO, 6-KS-3000, T-40 and JATO, 1.3-KS-4800, T-55 rocket motors, respectively.

The propulsion system for this investigation gave a maximum Mach number of 7.25 at an altitude of 47,000 feet; however, during the burning of the third-stage rocket motor the model assumed an angle of attack of undetermined magnitude and made it necessary to disregard data obtained after second-stage burning. Accelerometer data indicated the maximum model angle of attack to be less than ±0.50° over the period for which data are reported and was therefore neglected in the reduction and analysis of the data. Free-stream static pressure and temperature as obtained from radiosonde measurements, along with calculated stagnation temperature for the flight trajectory, are shown in figure 5. The variation of flight Mach number and free-stream Reynolds number per foot is shown in figure 6. The free-stream Reynolds number based on the various leading-edge diameters used is shown in figure 7.

DATA REDUCTION

Local Flow Conditions

Local flow conditions existing at the stagnation line and points around the cylindrical portion of each of the segments were calculated by using equations (10b), (10c), and (10d) of reference 4. A local pressure was measured on the 45° swept, 3/4-inch leading-edge-diameter segment at the station indicated in figure 3(a) and is presented in figure 8 as pressure coefficient. This pressure was used to obtain local values of Mach number and temperature on the flat surface by assuming isentropic expansion back from the stagnation line. The local conditions thus obtained were considered constant along the flat portion of the leading-edge segment and were also assumed to be the same for the other three leading-edge segments. Inasmuch as adiabatic wall temperature is a weak function of local temperature, it was felt that this approximation of assuming the same flat pressure on all segments would not affect experimental values of heat transfer to any great extent.

Adiabatic Wall Temperature, Wall Heating Rate,

and Heat-Transfer Coefficient

At the stagnation line of each leading-edge segment the adiabatic wall temperature was obtained by using the expression derived in reference 2 for a yawed cylinder. This expression based on free-stream temperature is

6

$$\frac{T_{aw} - T_\infty}{T_t - T_\infty} = 1 - \left(1 - N_{Pr}^{n}\right)\sin^2\Lambda$$

where $n = 1/2$ for laminar flow and $n = 1/3$ for turbulent flow. At points other than the stagnation line the relation for calculating T_{aw} was

$$\frac{T_{aw} - T_l}{T_t - T_l} = N_{Pr}^{n}$$

where again $n = 1/2$ or $1/3$ for laminar or turbulent flow, respectively. In all cases Prandtl number was evaluated at the outside surface temperature.

The temperature gradient through the wall was calculated from the measured time history of the inside wall temperatures by the method described in the appendix of reference 8. An average wall-temperature time history was obtained by integrating the temperature distribution through the wall at each time. The values of dT_w/dt were then computed by a five-point polynomial system by using an IBM 650 electronic data processing machine. These values were then used to calculate the wall-heating rate by the relation

$$q = \rho_w c_w \tau \frac{dT_w}{dt}\left(1 - \frac{\tau}{D}\right)$$

where c_w was evaluated at the average wall temperature. The local heat-transfer coefficients per unit area were calculated by the relation

$$h = \frac{1}{T_{aw} - T_s}\left[\rho_w c_w \tau \frac{dT_w}{dt}\left(1 - \frac{\tau}{D}\right) + q_{conduction}\right]$$

where T_s is the calculated outside surface temperature.

Calculations were made of the amount cf heat lost by chordwise conduction at the stagnation line for each leading-edge segment. This was done by analytically dividing the cylindrical portion of the leading edges into a number of small blocks as illustrated in the following sketch.

Row 2

Row 1
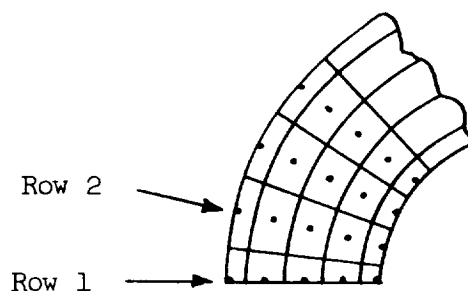
Heat-balance equations were written for each block based on the method of Dusinberre as found in reference 10. Experimental values of heat-transfer coefficient for the stagnation line were used and these values were assumed to decrease around the leading edge according to the order described in reference 4. The heat-balance equations were then solved simultaneously for the temperature of each block. The heat lost by each block at the stagnation line, row 1, to its adjacent block in row 2 was then calculated and totaled to obtain the total heat lost at the stagnation line at any one time. The amount of heat lost by conduction as calculated for each segment, except the 1/4-inch leading-edge-diameter segment, was found to be less than 5 percent of the measured heating rate and was neglected. The heat lost by conduction at the stagnation line of the 1/4-inch leading-edge-diameter segment was calculated to be approximately 6 percent and 15 percent of the measured heat transfer in the time ranges 2.0 to 3.2 and 52.0 to 56.0 seconds, respectively. This correction was added to the experimental values of heating rate. No corrections were made for the heat lost by radiation as this quantity was found to be negligible in the wall temperature range of this investigation.

The estimated maximum error in the level of the measured wall temperature was about 22°. The change in temperature with time is much more accurate than this as several successive data points are involved in the fairing process used to evaluate dT/dt. Calculations using the various quantities involved indicate the Stanton numbers presented are accurate to within ± 15 percent.

RESULTS AND DISCUSSION

Pressure Coefficient

The pressure coefficients measured on the flat portion of the $\Lambda = 45^\circ$, 3/4-inch-diameter segment are shown in figure 8. The negative pressure coefficients indicate overexpansion of the air around the

leading edge. This condition seems reasonable because of the relative closeness of the measurement station to the blunt leading edge. The values are essentially in agreement with pressure measurements in reference 8 when correlated on a basis of normal Mach number.

A small shift in model angle of attack at $t = 2.6$ seconds was indicated by accelerometer measurements, which would explain the shift in measured pressure coefficient at this time. Again, it is pointed out that accelerometer measurements indicated the maximum angle of attack was within $\pm 0.50°$ during the period for which data are reported.

Skin Temperature

Because of the relatively high heating rates and low thermal conductivity of the wall material, it was necessary to calculate temperature gradients through the wall to determine accurately the heat transfer as described under the section entitled "Data Reduction." Values of measured inside surface temperatures for all measurement stations are shown in figure 9. Figure 10 shows the measured inside surface and calculated outside surface temperatures for a typical thermocouple location. Temperature-gradient calculations were started at times $t = 1.0$ second and 50.0 seconds to obtain accurate values of temperature gradient during the data-reporting periods. Temperature and heat-transfer data are not presented at these earlier times as the change in wall temperature with time was not of sufficient magnitude to determine accurately the wall-heating rates.

Heat Transfer

The heat-transfer data are presented as nondimensional Stanton number based on free-stream conditions. It was felt that local conditions at each thermocouple location were not well enough defined to warrant their use as a basis for Stanton number. The Stanton number for each thermocouple location on all leading-edge segments is presented in subsequent figures where they are considered in systematic groups.

Comparison with theory at the stagnation line.- Figure 11 shows the comparison of experimental and theoretical Stanton number for the stagnation line of each leading-edge segment. The local conditions used in these theories were those calculated by using equations (10b), (10c), and (10d) of reference 4. In the time range from 2.0 to 3.2 seconds, the experimental values of heat transfer were found to be considerably higher than those predicted by the laminar theory of reference 4. As mentioned previously, it is shown in references 6 to 8 that at high Reynolds numbers it is possible to obtain values of heat transfer on swept leading edges much higher than those predicted for a laminar boundary layer. It was

believed that this increase was caused by sweep influencing the boundary layer to such an extent that at high sweep angles the boundary layer became turbulent. Recent work by Beckwith and Gallagher (ref. 7) presents a theory for calculating local heat transfer at points around a yawed cylinder in the presence of a turbulent boundary layer. The values of heat transfer obtained by using this theory are shown in figure 11.

This comparison between experimental and theoretical values of heat transfer for both the $\Lambda = 45^\circ$ and $\Lambda = 36.75^\circ$ segments (figs. 11(a) to 11(d)) indicates that the boundary layer at the stagnation line of each segment was of a transitional nature. Increasing the leading-edge diameter from 1/4 inch to 3/4 inch for the $\Lambda = 45^\circ$ segments (figs. 11(a) to 11(c)) caused no appreciable change in the magnitude of the experimental heat transfer at the stagnation line. However, since the theoretical Stanton number changes with diameter it appears that the boundary layer at the stagnation line was approaching a more fully turbulent state as the leading-edge diameter was increased.

In the time range 52.0 to 56.0 seconds the experimental heat transfer for the $\Lambda = 45^\circ$, 3/4-inch-diameter segment (fig. 11(e)) is slightly higher than that predicted by turbulent theory. For the 1/2-inch-diameter, $\Lambda = 45^\circ$ and 36.75° segments (figs. 11(f) and 11(h)) it is difficult to determine the character of flow from a comparison of the experimental and theoretical magnitudes. However, the trend of the experimental values, that is, the rapid increase with time, indicates transition to turbulent flow along the leading edge of these segments. Experimental heat transfer for the $\Lambda = 45^\circ$, 1/4-inch-diameter segment (fig. 11(g)) falls on an average about 35 percent below the values predicted by both laminar and turbulent theories. This order of magnitude and the relatively small change in heat transfer with time indicate the boundary layer at the stagnation line of this segment was probably of a laminar nature. This change from laminar to turbulent flow with an increase in leading-edge diameter suggests an effect of Reynolds number based on leading-edge diameter. It appears from this low Reynolds number data (figs. 11(e) to 11(h)) that the critical Reynolds number based on leading-edge diameter is in the range covered by the 1/2-inch-diameter segment (0.11×10^6 to 0.17×10^6). This result is in very good agreement with the results of reference 6 where a transition Reynolds number R_D of 0.18×10^6 for a sweep angle of 39.7° was noted. However, this result is not in agreement with the higher Reynolds number data (figs. 11(a) to 11(d)) where experimental heat transfer was not fully turbulent for values of R_D several times greater than 0.17×10^6 even though Mach number conditions were similar.

Comparison with theory back of stagnation line.- Experimental heat transfer for stations back of the stagnation line is compared with laminar- and turbulent-theory predictions in figure 12. For stations

on the flat portions of the leading-edge segments (figs. 12(b) to 12(f) and 12(h) and 12(ι)), the laminar theory used is that found in reference 11 and the turbulent theory is that found in references 12 and 13. In each case a value of 0.6 was assumed for the ratio of Stanton number to skin-friction coefficient. The length used in the calculations was the wetted length measured in a streamwise direction from the stagnation line. The necessary local conditions were calculated by using pressures measured on the flat portion of the 45° sweep $3/4$-inch-diameter segment and by assuming isentropic expansion from the stagnation line. In the time range from 2.0 to 3.2 seconds (figs. 12(a) to 12(f)), the experimental heat transfer shows reasonably good agreement with values predicted by turbulent theory with the exception of the 36.75° sweep, 0.312 chord station (fig. 12(e)). It is felt the heat transfer at this station, located at the cylinder-flat juncture, was being influenced by conduction. The magnitude of the chordwise conduction could not be estimated as the heat-transfer coefficient in the immediate vicinity of this station was not known.

In the time range from 52.0 to 56.0 seconds at the $\Phi = 45^\circ$ station of the 45° sweep, $3/4$-inch-diameter segment (fig. 12(g)) the experimental values of heat transfer are on an average approximately 20 percent higher than those predicted by turbulent theory. At the other measurement stations, except the 36.75° sweep, 0.312 chord station, the experimental heat transfer agrees very well with laminar predictions. At this station on the 36.75° sweep segment (fig. 12(k)) the experimental heat transfer increases steadily from laminar to greater than turbulent predictions. As mentioned previously, it is felt that the location of this measurement station caused the heat transfer to be affected by conduction to an extent that no conclusion as to the type of flow at this station can be made.

Chordwise distribution of heat transfer.- The heat-transfer data of figures 11 and 12 have been combined and plotted in figure 13 as a function of chordwise distance for each leading-edge segment. The values of theoretical heat transfer are shown plotted as bands to give an idea of the range rather than specific values. Observation of the turbulent theory bands indicates a discontinuity at the cylinder-flat juncture, whereas the laminar theory bands are more nearly coincident in this region. It is felt that the variation of theoretical turbulent heat transfer should vary smoothly from the cylinder to the flat portion if no flow separation occurs. This condition indicates the turbulent theory underestimates heat transfer at large azimuth angles around the cylindrical portion of the leading-edge segments. It is noted that in the low Reynolds number region (figs. 13(e) to 13(h)) turbulent theory predicts values of heat transfer to the cylindrical portion of the leading edges which are in some cases lower than values predicted by laminar theory. It is felt that in such cases the turbulent theory has been extended into a region where its applicability is in question.

In the previous discussion it was pointed out that for the time range from 2.0 to 3.2 seconds the heat transfer was transitional or turbulent, depending on the particular segment, at the stagnation line and turbulent at all stations downstream. This result is more clearly seen in figures 13(a) to 13(d). For the time range 52.0 to 56.0 seconds it was shown that the heat transfer was laminar, transitional, or turbulent, depending on the particular segment, on the cylindrical portion of the leading-edge segments. However, in each case the flow over the flat portion of the segments downstream of the cylinder-body juncture appeared to be laminar. This variation can also be seen in figures 13(e) to 13(h). This difference in flow region indicates at sufficiently low values of R_D a transitional or turbulent boundary layer can exist at the stagnation line while laminar flow exists downstream of the blunted portion of the leading edge. It is pointed out that this disturbance might extend downstream from the leading edge at points farther outboard than where measurements were made.

Effect of sweep.- The effect of sweep on the heat transfer to the stagnation line for a 3/4-inch-diameter leading-edge segment is shown in figure 14. The data of reference 8 and the present tests were used to provide points at $\Lambda = 0^\circ$, 45°, and 75° for $M = 2.99$. The theoretical variation of the laminar heat transfer with sweep angle shown is that calculated by use of reference 4. It is pointed out that the heat transfer of reference 8 ($\Lambda = 0^\circ$ and $\Lambda = 75^\circ$) was believed to be higher than laminar theory predicted because of body-interference effects present in the case of $\Lambda = 0^\circ$ and because of boundary-layer transition in the case of $\Lambda = 75^\circ$. It is felt that the heat transfer to the 45° segment of the present test was being influenced by boundary-layer transition resulting in heating greater than laminar predictions.

Spanwise variation of heat transfer.- Measurements were made of heat transfer along the stagnation line of each segment to determine whether the measurements made were out of the field of influence of the model body. Observation of the data of figure 11 shows only random variation of heat transfer with spanwise distance, no one station showing any consistent trend of increased or decreased heating. The maximum spread of heat-transfer values presented is within the experimental accuracy of the data. The boundary-layer thickness on the model body in the vicinity of the leading-edge segments was calculated and was found to vary from 0.44 to 0.40 inch in the time range 2.0 to 3.2 seconds and from 0.60 to 0.54 inch in the time range 52.0 to 56.0 seconds. The values of boundary-layer thickness all lie within the most inboard measuring station $b = 0.75$ inch. It is felt that the heat-transfer data presented are representative of free-stream values insofar as no consistent localized high heat transfer at the more inboard stations was observed.

CONCLUSIONS

A flight investigation has been conducted to measure the heat transfer to swept leading-edge segments of various degrees of bluntness. The leading-edge segments were cylindrically blunted wedges, three of which were swept 45° with leading-edge diameters of 1/4, 1/2, and 3/4 inch and one swept 36.75° with a leading-edge diameter of 1/2 inch. This investigation covered Mach number ranges of 1.78 to 2.99 and 2.50 to 4.05 with corresponding free-stream Reynolds numbers per foot ranges of 13.32×10^6 to 19.90×10^6 and 2.85×10^6 to 4.55×10^6. Conclusions drawn from the results of this investigation are:

In the high Reynolds number range, measured values of heat transfer were found to be much higher than those predicted by laminar theory and at the larger values of leading-edge diameter were approaching the values predicted by turbulent theory. For the low Reynolds number range a comparison between measured and theoretical heat transfer showed that increasing the leading-edge diameter induced turbulent flow on the cylindrical portion of the leading edge.

Langley Research Center,
    National Aeronautics and Space Administration,
        Langley Field, Va., September 18, 1959.

REFERENCES

1. Reshotko, Eli, and Cohen, Clarence B.: Heat Transfer at the Forward
     Stagnation Point of Blunt Bodies. NACA TN 3513, 1955.

2. Reshotko, Eli: Heat Transfer to a Yawed Infinite Cylinder in Com-
     pressible Flow. 1956 Heat Transfer and Fluid Mechanics Inst.,
     Stanford Univ. (Stanford, Calif.), June 21-23, 1956, pp. 205-220.

3. Beckwith, Ivan E.: Theoretical Investigation of Laminar Heat Transfer
     on Yawed Infinite Cylinders in Supersonic Flow and a Comparison With
     Experimental Data. NACA RM L55F09, 1955.

4. Goodwin, Glen, Creager, Marcus O., and Winkler, Ernest L.: Investiga-
     tion of Local Heat-Transfer and Pressure Drag Characteristics of a
     Yawed Circular Cylinder at Supersonic Speeds. NACA RM A55H31, 1956.

5. Feller, William V.: Investigation of Equilibrium Temperatures and
     Average Laminar Heat-Transfer Coefficients for the Front Half of
     Swept Circular Cylinders at a Mach Number of 6.9. NACA RM L55F08a,
     1955.

6. Beckwith, Ivan E., and Gallagher, James J.: Experimental Investigation
     of the Effect of Boundary-Layer Transition on the Average Heat Trans-
     fer to a Yawed Cylinder in Supersonic Flow. NACA RM L56E09, 1956.

7. Beckwith, Ivan E., and Gallagher, James J.: Local Heat Transfer and
     Recovery Temperatures on a Yawed Cylinder at a Mach Number of 4.15
     and High Reynolds Numbers. NASA MEMO 2-27-59L, 1959.

8. O'Neal, Robert L., and Bond, Aleck C.: Heat Transfer to 0° and 75°
     Swept Blunt Leading Edges in Free Flight at Mach Numbers From 1.90
     to 3.07. NACA RM L58A13, 1958.

9. Rumsey, Charles B., and Lee, Dorothy B.: Measurements of Aerodynamic
     Heat Transfer and Boundary-Layer Transition on a 15° Cone in Free
     Flight at Supersonic Mach Numbers Up to 5.2. NACA RM L56F26, 1956.

10. McAdams, William H.: Heat Transmission. Third ed., McGraw-Hill Book
     Co., Inc., 1954.

11. Van Driest, E. R.: Investigation of Laminar Boundary Layer in Com-
     pressible Fluids Using the Crocco Method. NACA TN 2597, 1952.

12. Van Driest, E. R.: The Turbulent Boundary Layer for Compressible
     Fluids on a Flat Plate With Heat Transfer. Rep. No. AL-997, North
     American Aviation, Inc., Jan. 27, 1950.

14

13. Van Driest, E. R.: The Turbulent Boundary Layer With Variable
    Prandtl Number. Rep. No. AL-1914, North American Aviation, Inc.,
    Apr. 2, 1954.
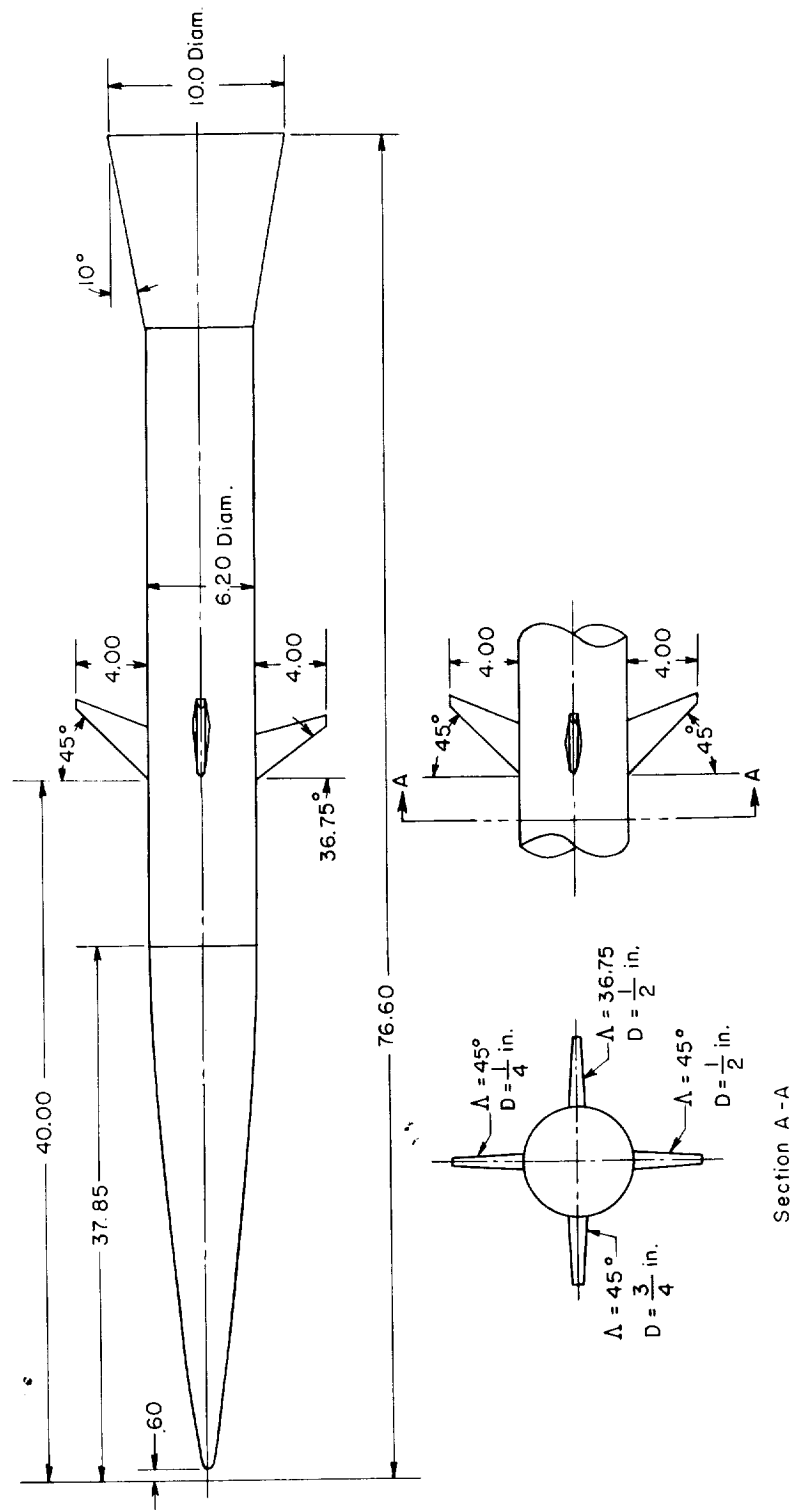
Figure 1.- Sketch of test vehicle showing location of wing leading-edge segments. All dimensions are in inches unless otherwise noted.
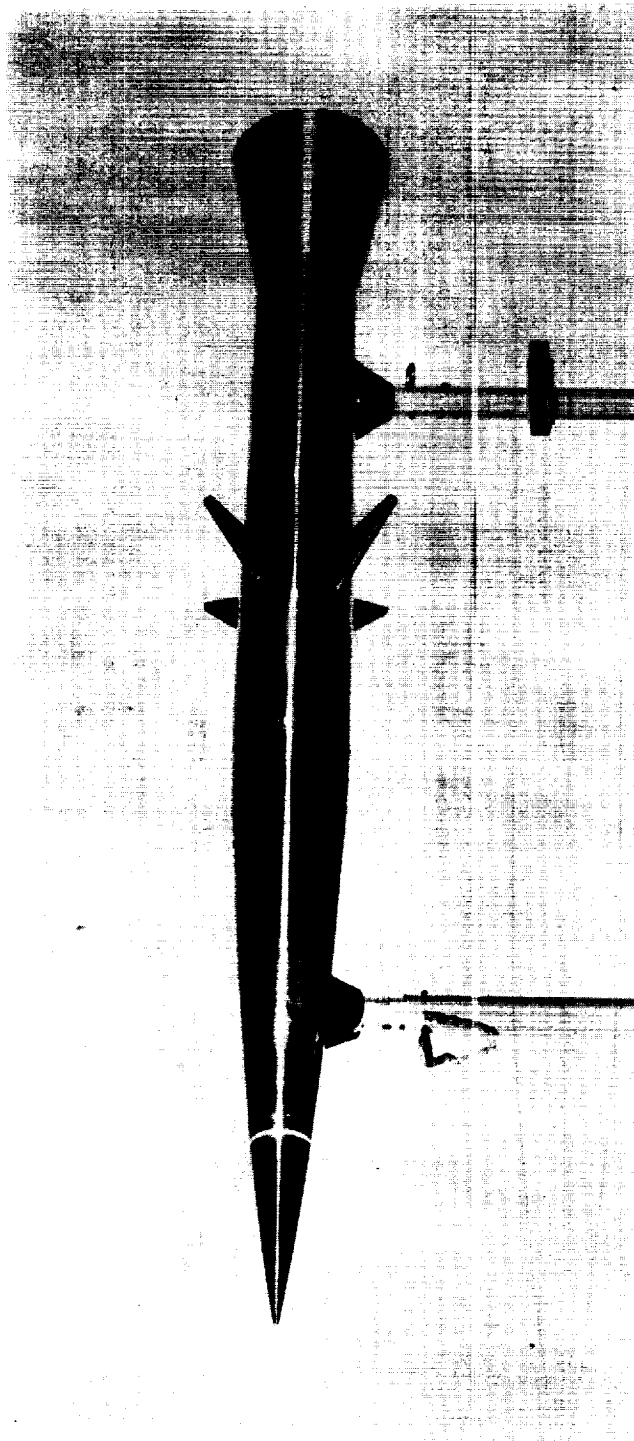
Figure 2.- Model used in the investigation.   L-57-5137

Typical section
perpendicular to
leading edge

Fuselage wall

Resin filler block

$D = \frac{3}{4}$ in.

$D = \frac{1}{2}$ in.

$D = \frac{1}{4}$ in.

Section A-A,D-D

Section A-A,C-C,D-D

Section A-A,C-C,D-D

Section B-B

Section B-B

Section B-B

Pressure orifice

Denotes thermocouple

Section C-C

(a) $\Lambda = 45^{\circ}$.
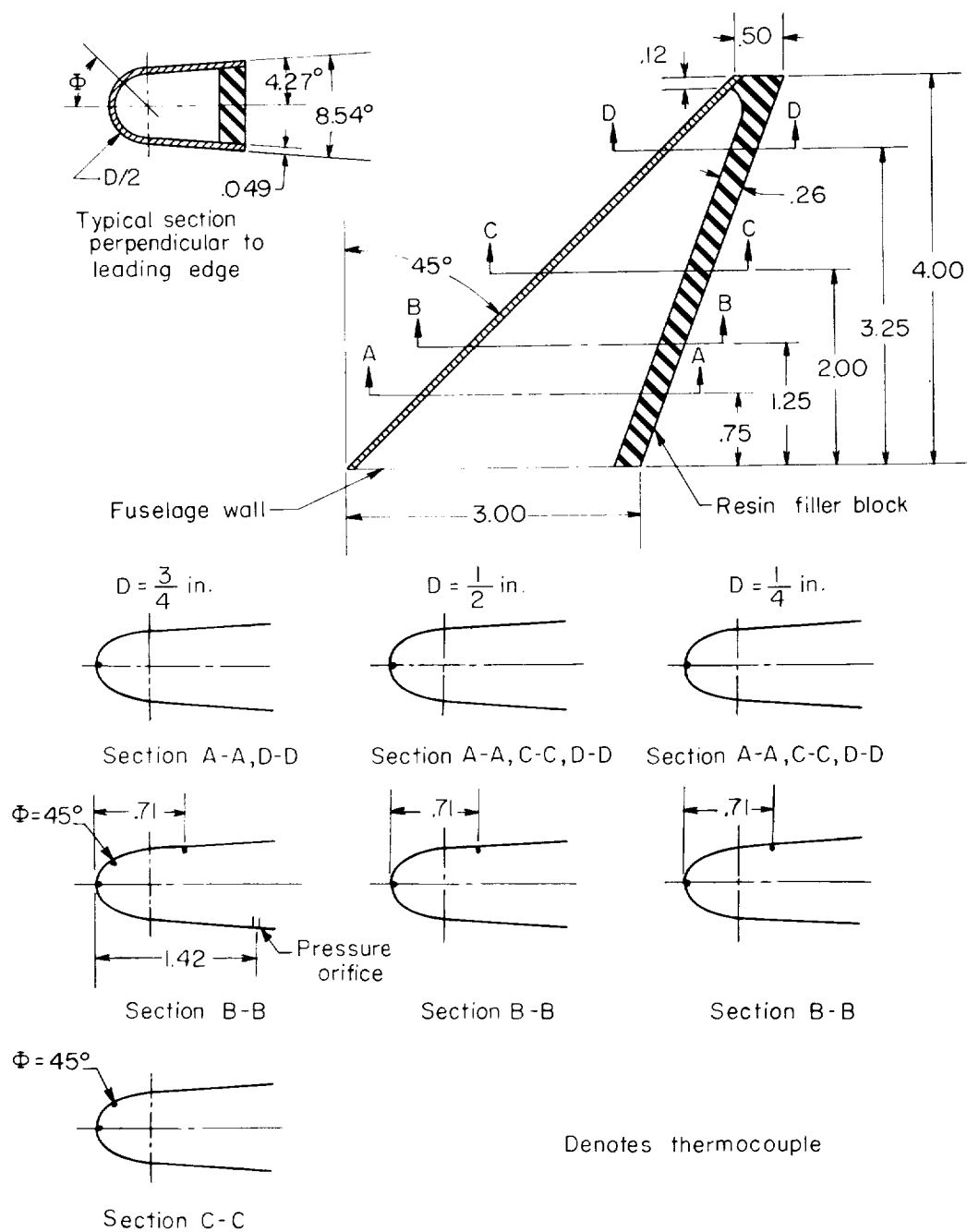
Figure 3.- Sketch of wing leading-edge segments showing thermocouple
locations. All dimensions are in inches unless otherwise noted.

Typical section
perpendicular to
leading edge

Fuselage wall

$D = \frac{1}{2}$ in.

Section A-A, C-C, D-D

Section B-B
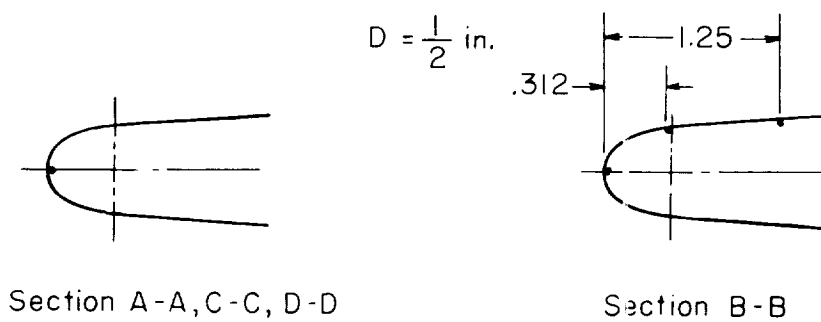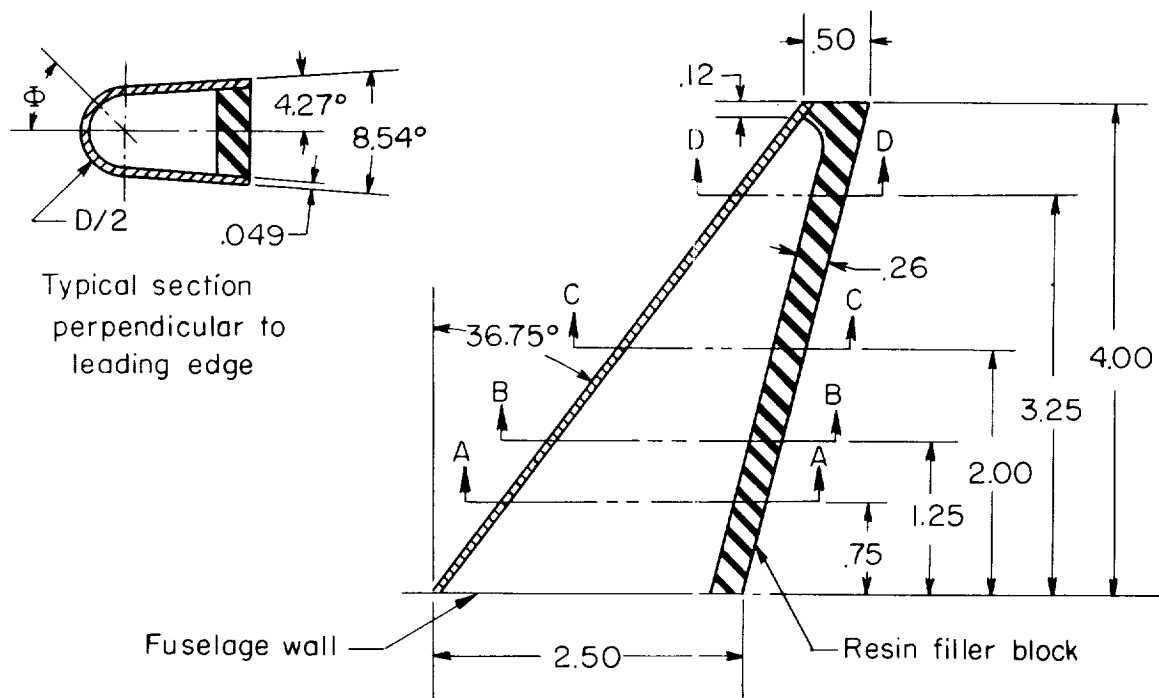
• Denotes thermocouple

(b) $\Lambda = 36.75°$.

Figure 3.- Concluded.
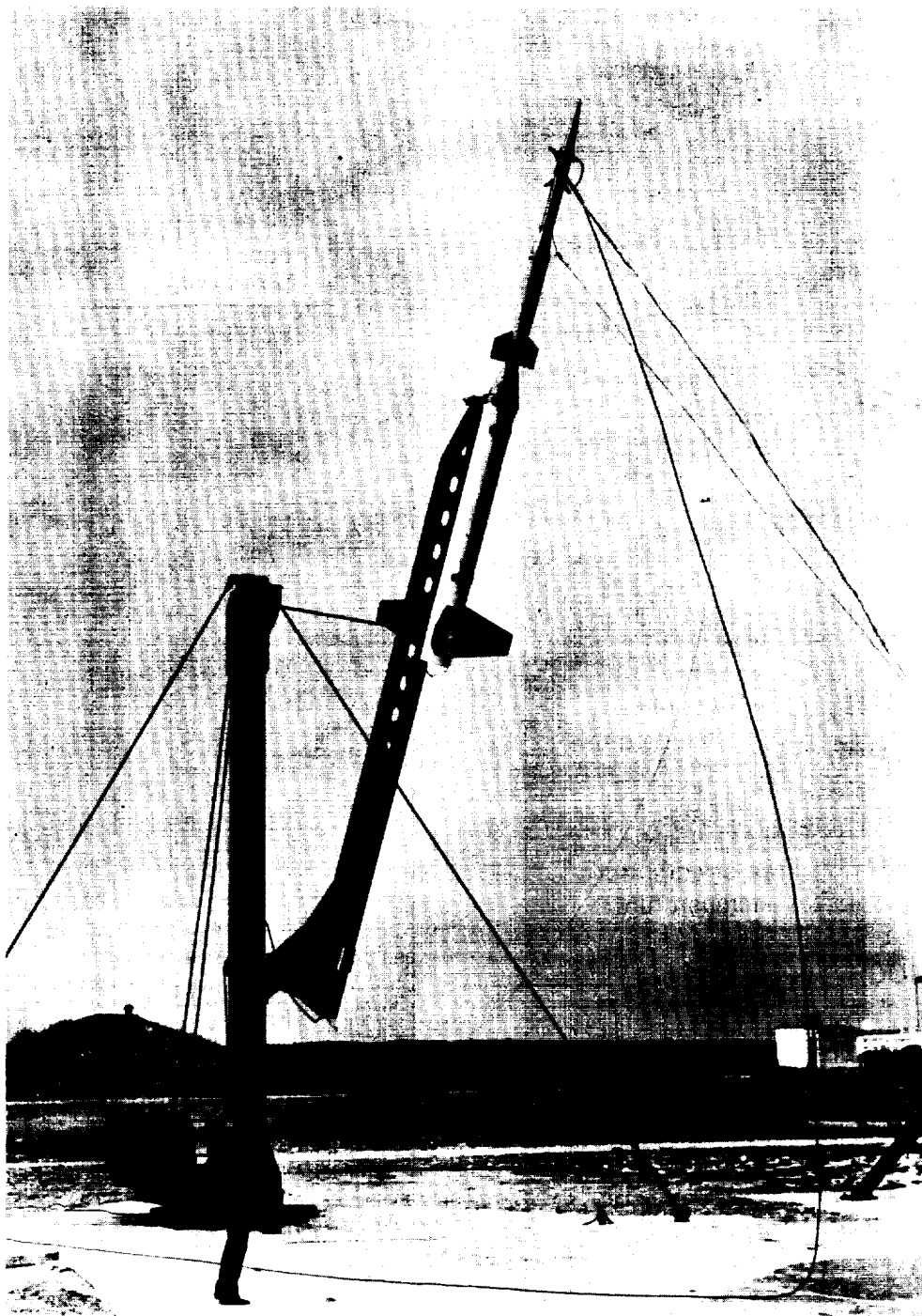
Figure 4.- Model and boosters on launcher. L-57-5622
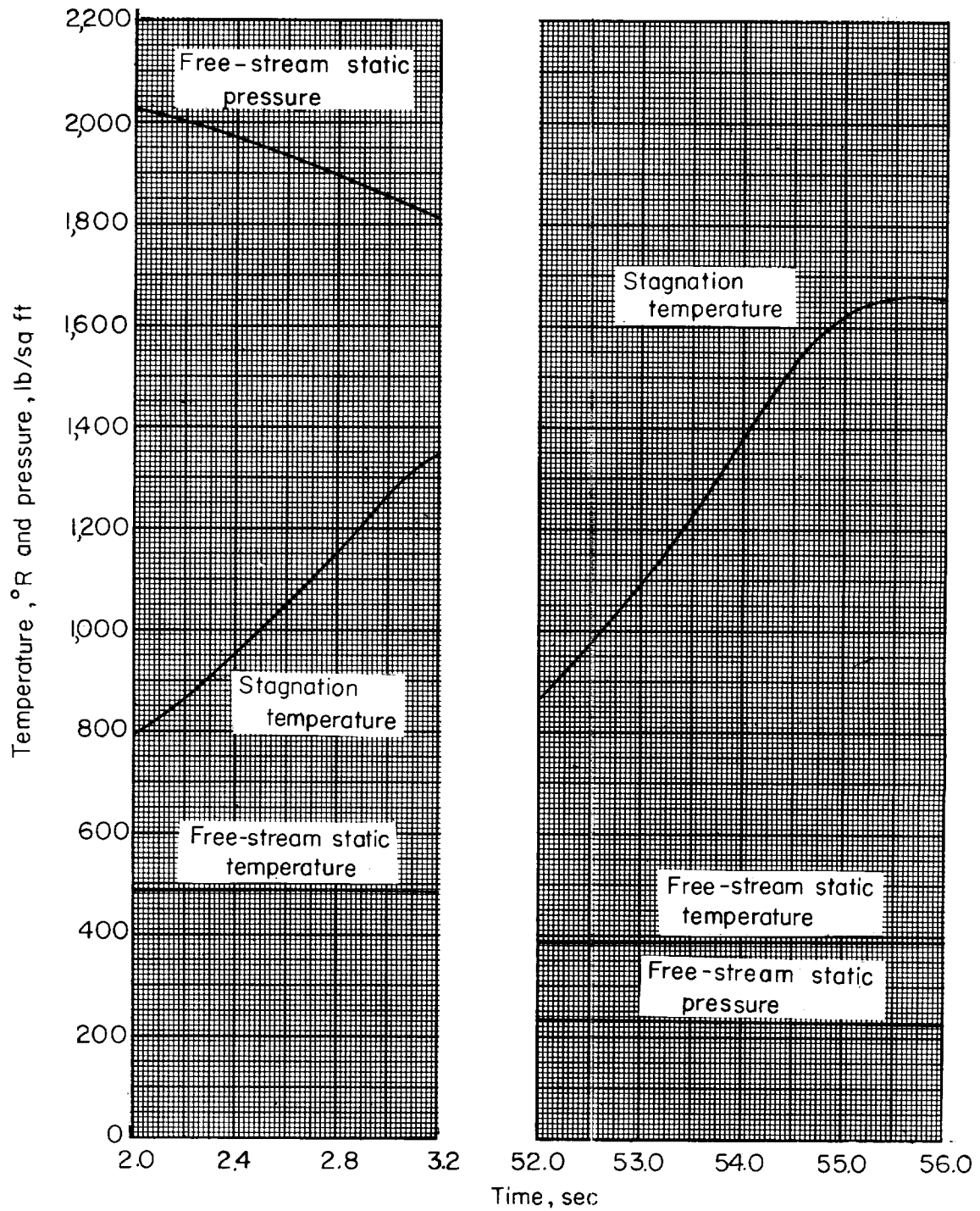
Figure 5.- Free-stream static temperature and pressure and stagnation
temperature for model flight trajectory.
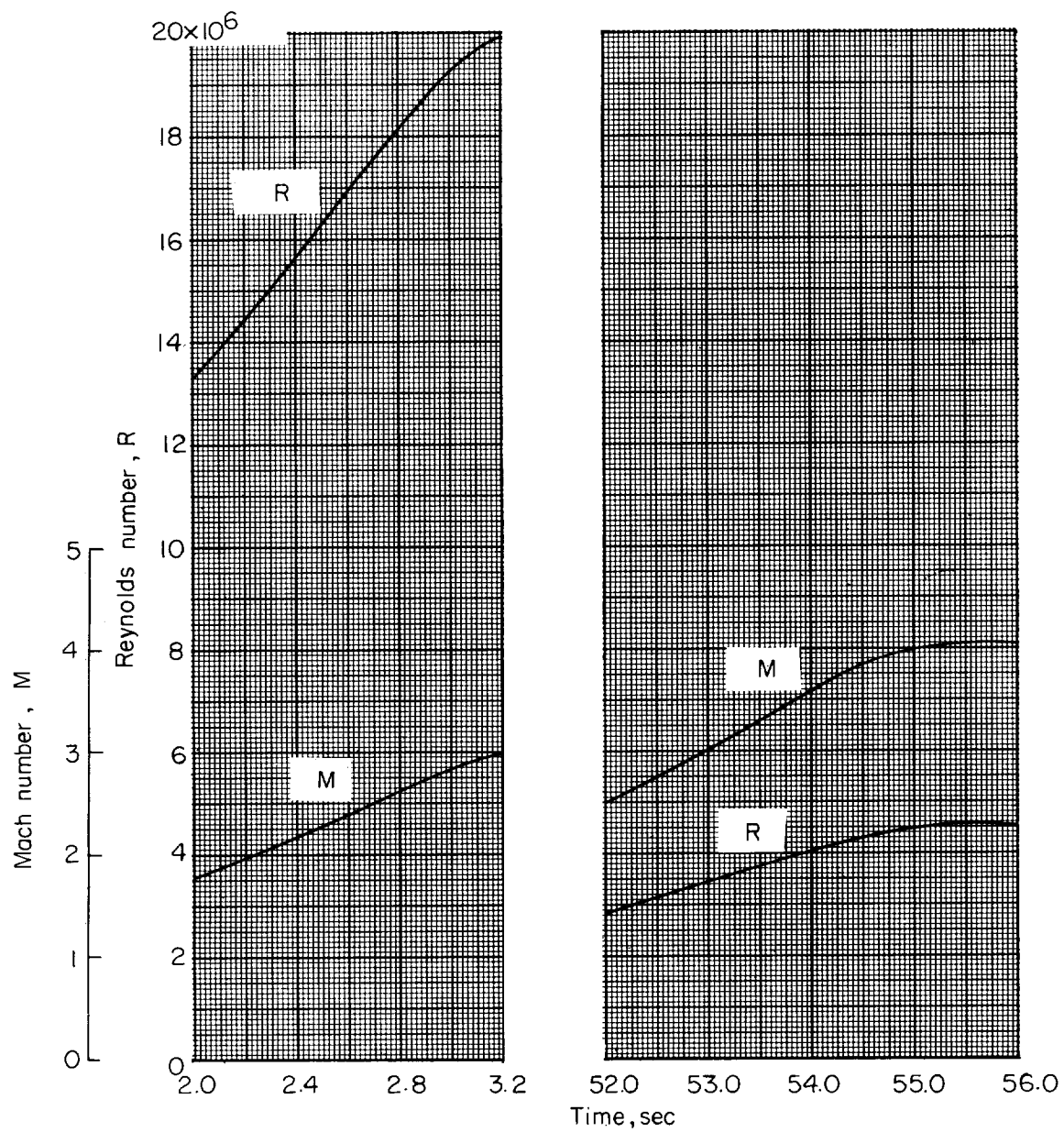
Figure 6.- Free-stream Mach number and Reynolds number (based on
1 foot).
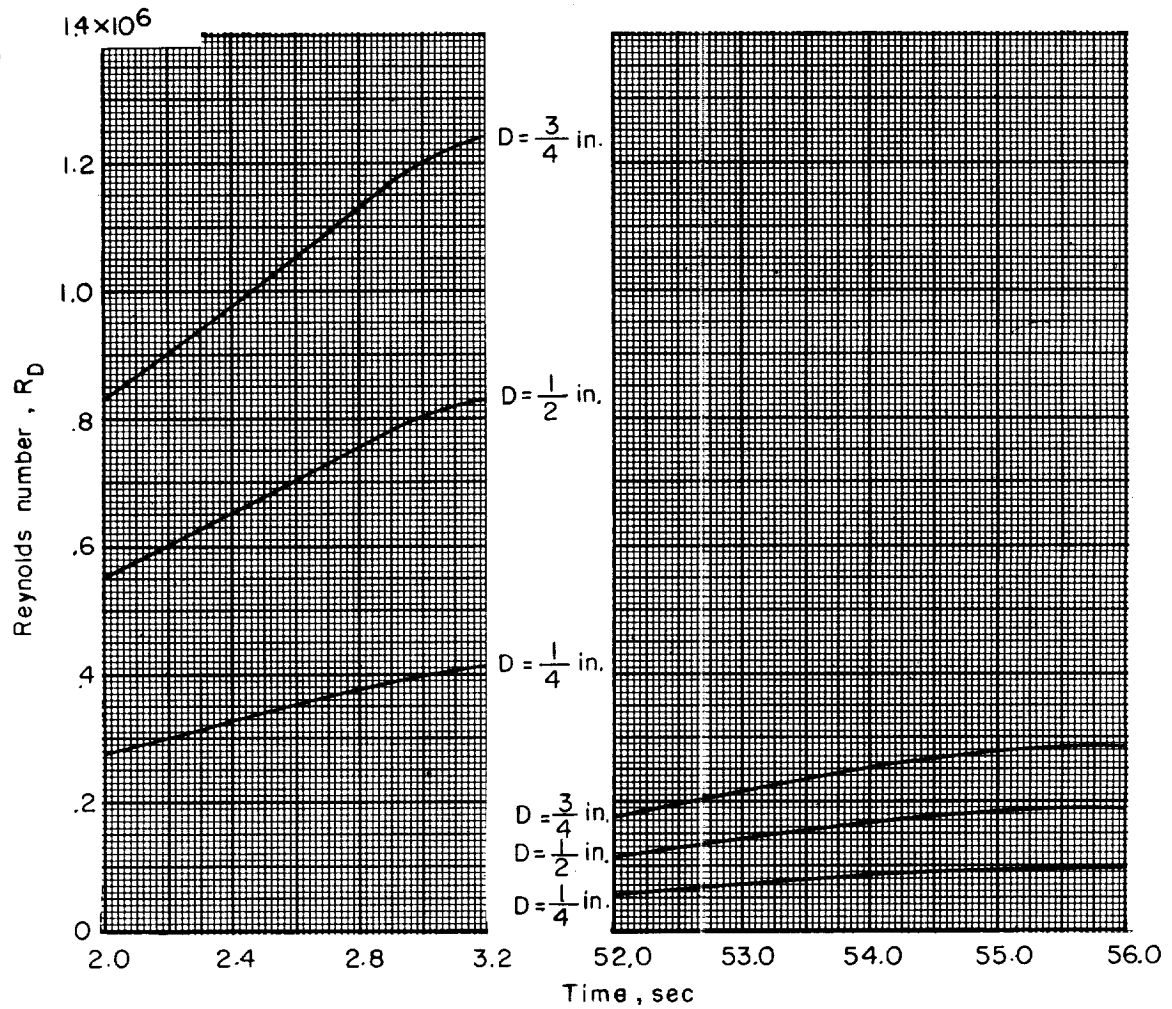
Figure 7.- Free-stream Reynolds number based on leading-edge diameter.
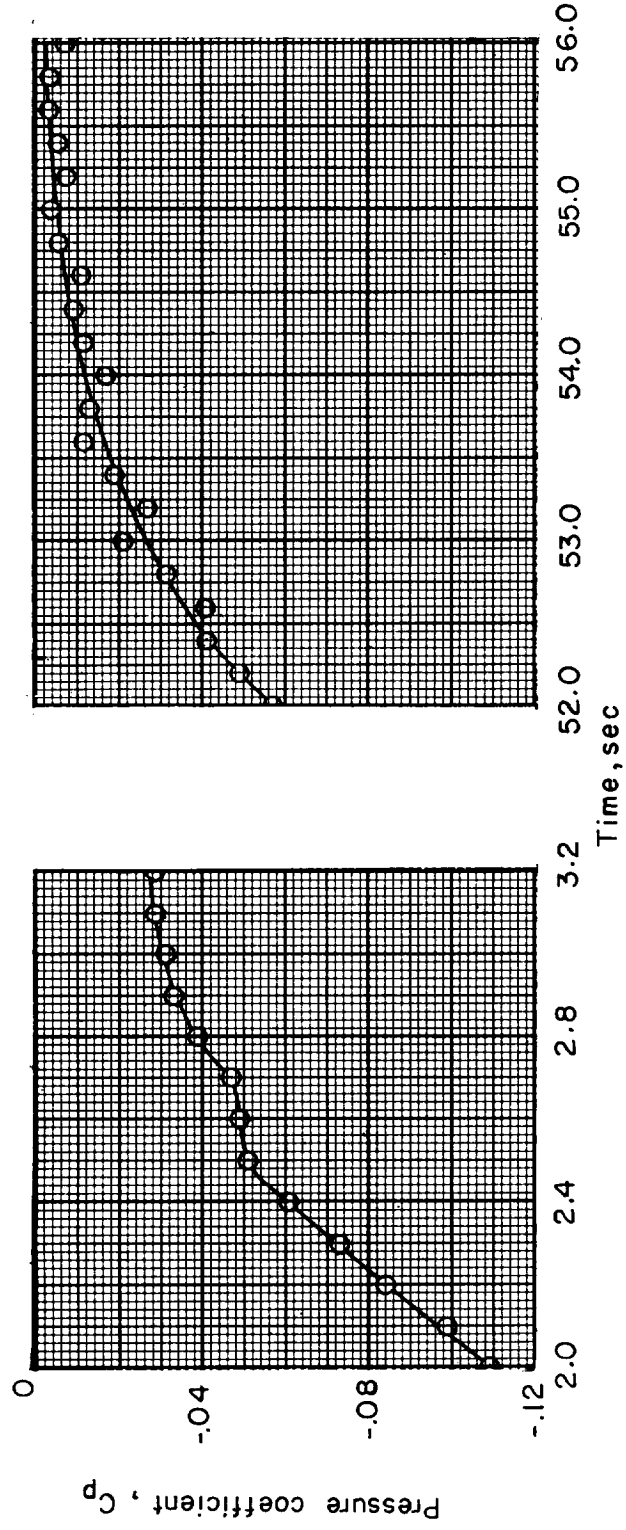
Figure 8.- Pressure coefficient measured on the 45° sweep, 3/4-inch-diameter leading-edge segment.
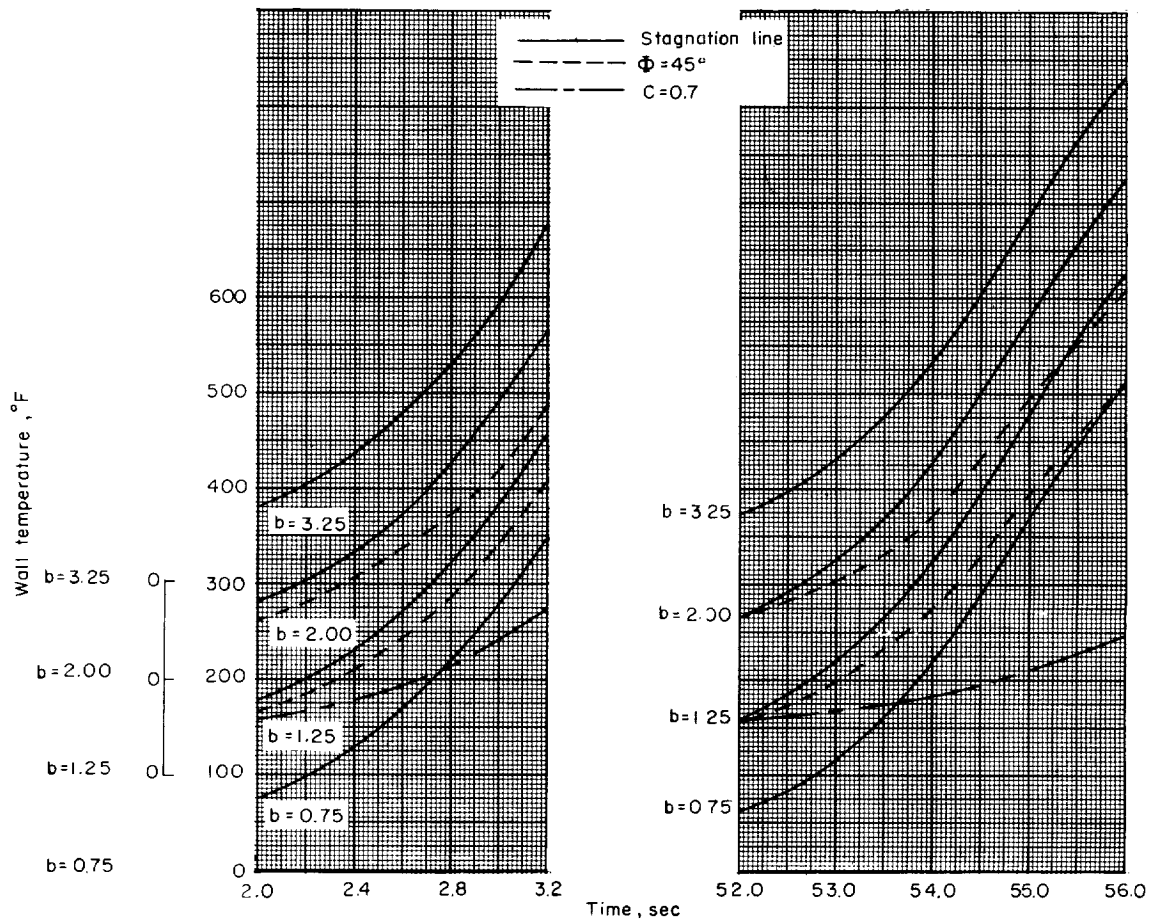
(a) $\Lambda = 45^\circ$; $D = \frac{3}{4}$ inch.

Figure 9.- Measured temperatures on leading-edge segments.
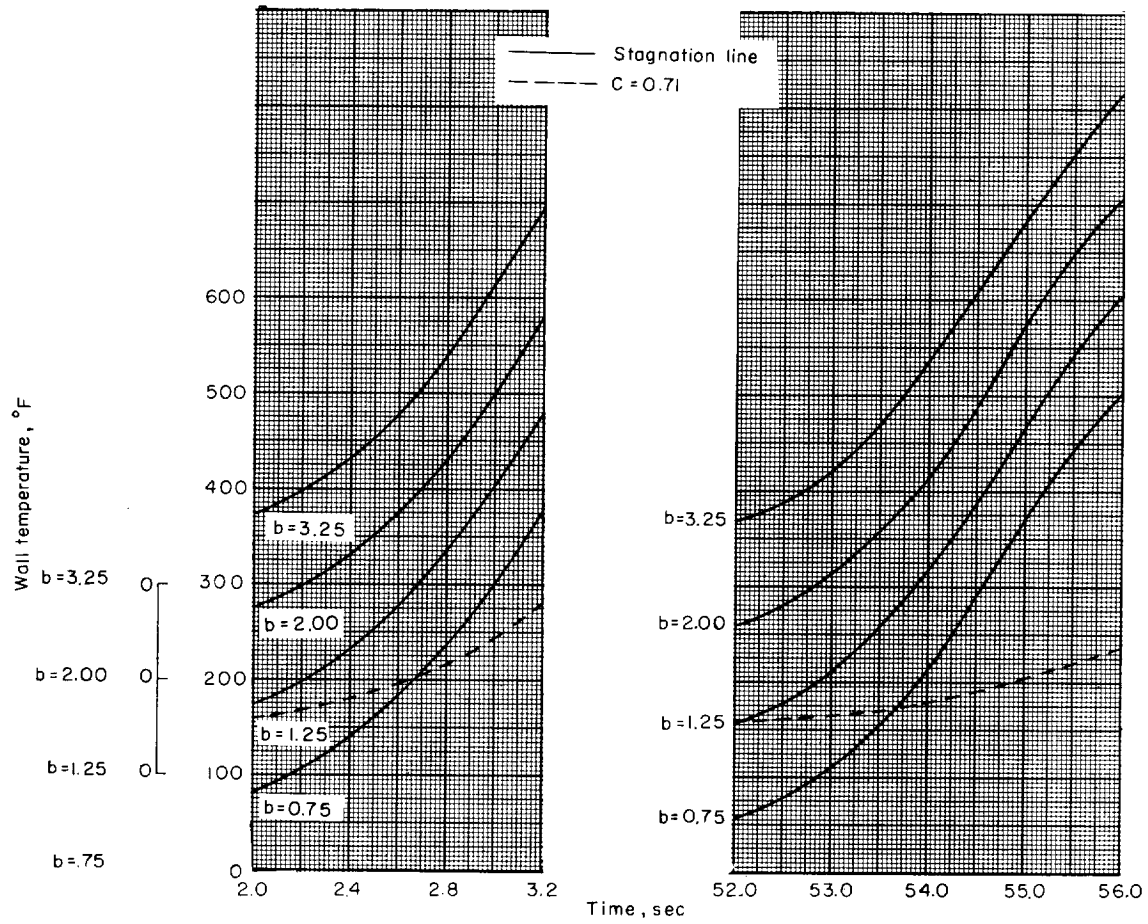
(b) $\Lambda = 45°$; $D = \frac{1}{2}$ inch.

Figure 9.- Continued.
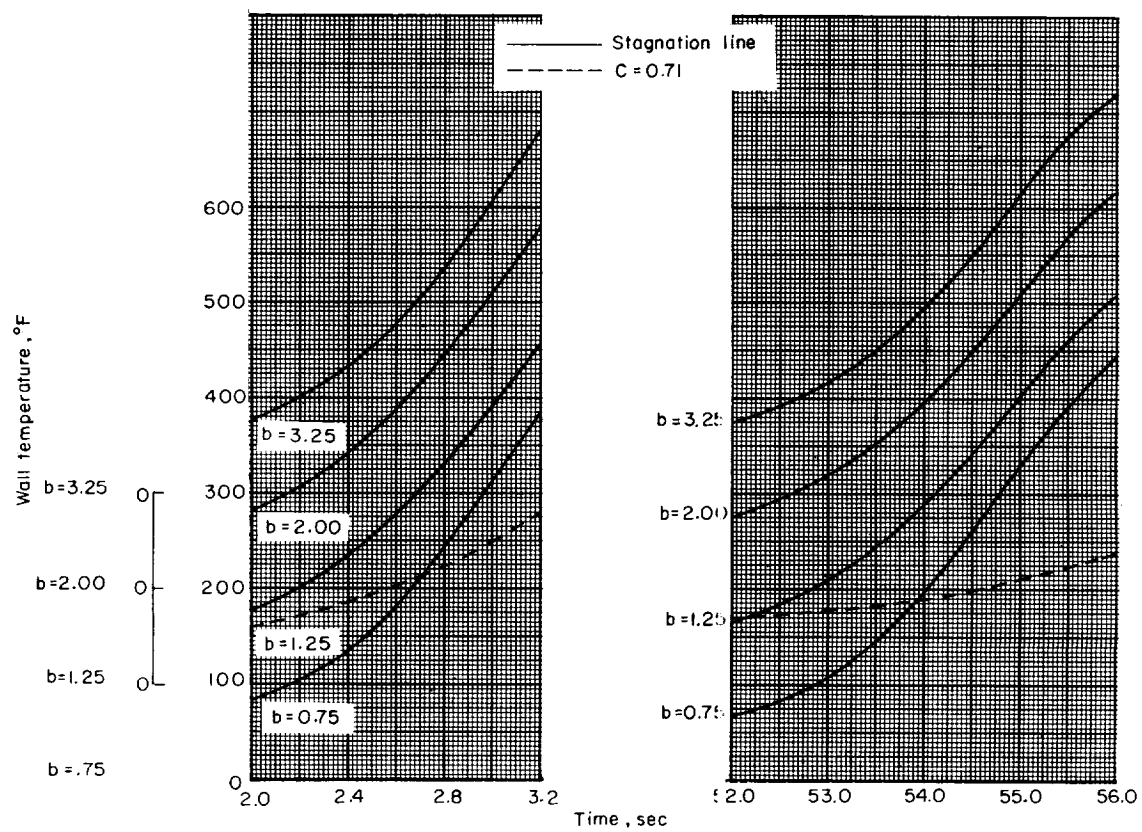
(c) $\Lambda = 45^\circ$; $D = \frac{1}{4}$ inch.

Figure 9.- Continued.
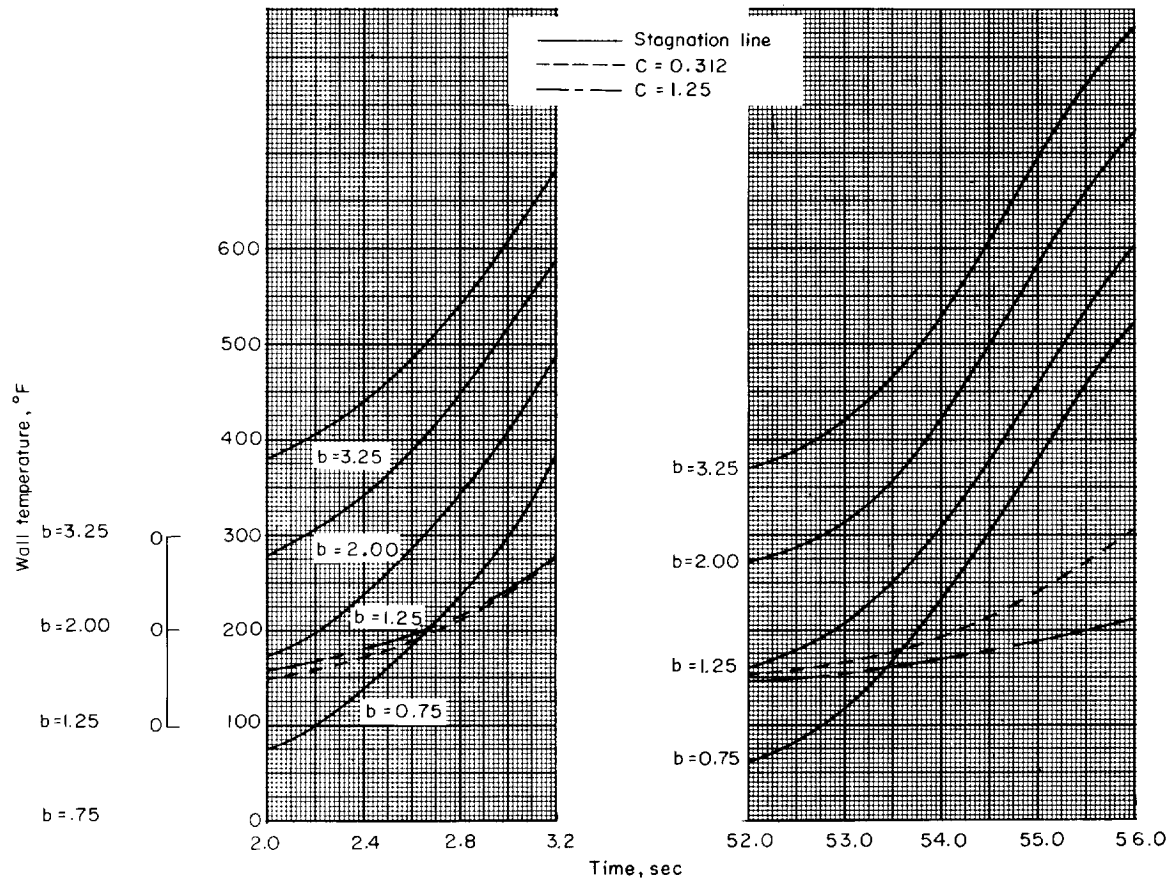
(d) $\Lambda = 36.75^{\circ}$; $D = \frac{1}{2}$ inch.

Figure 9.- Concluded.
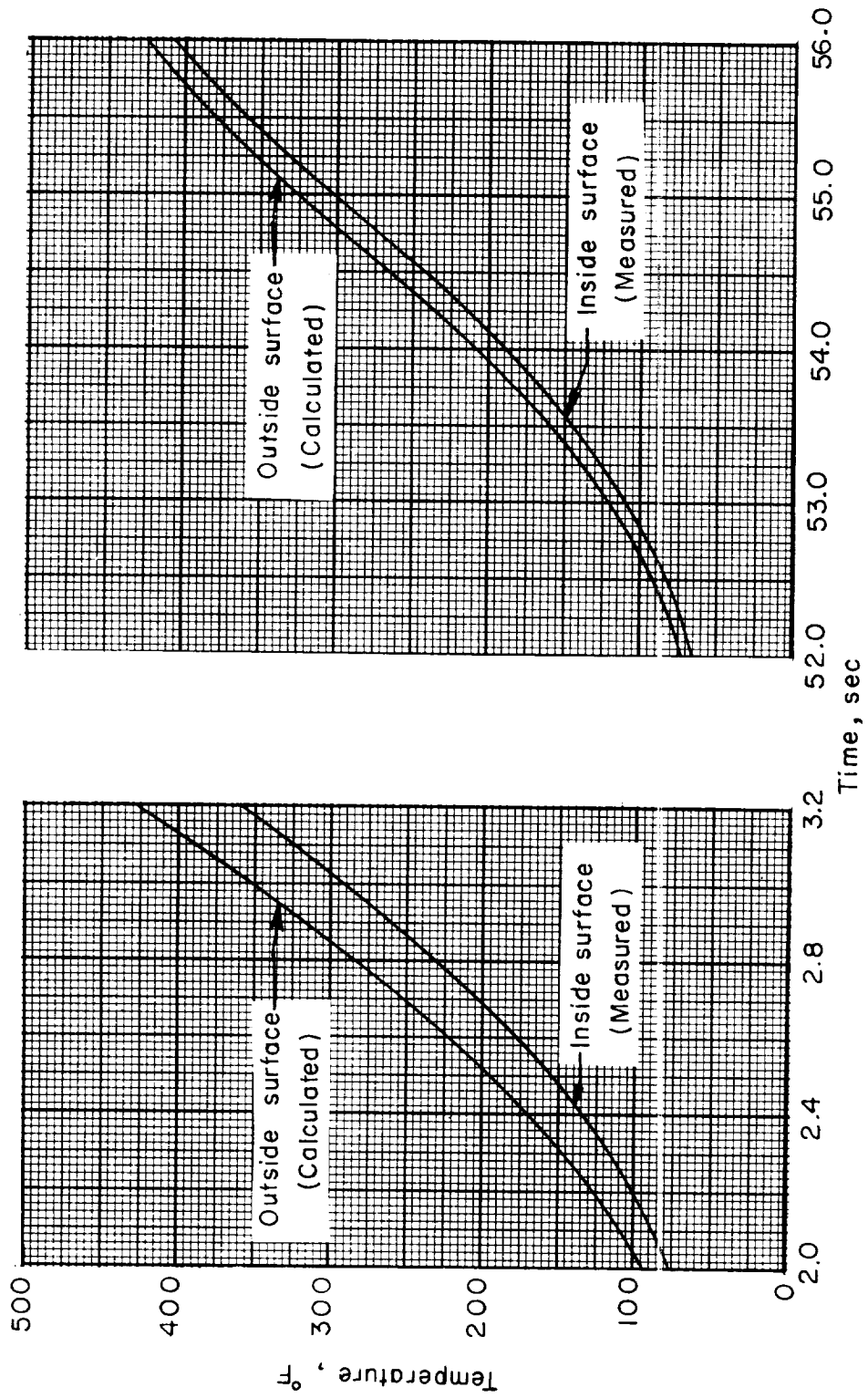
Figure 10.- Comparison of inside and outside surface temperatures for a typical thermocouple location.
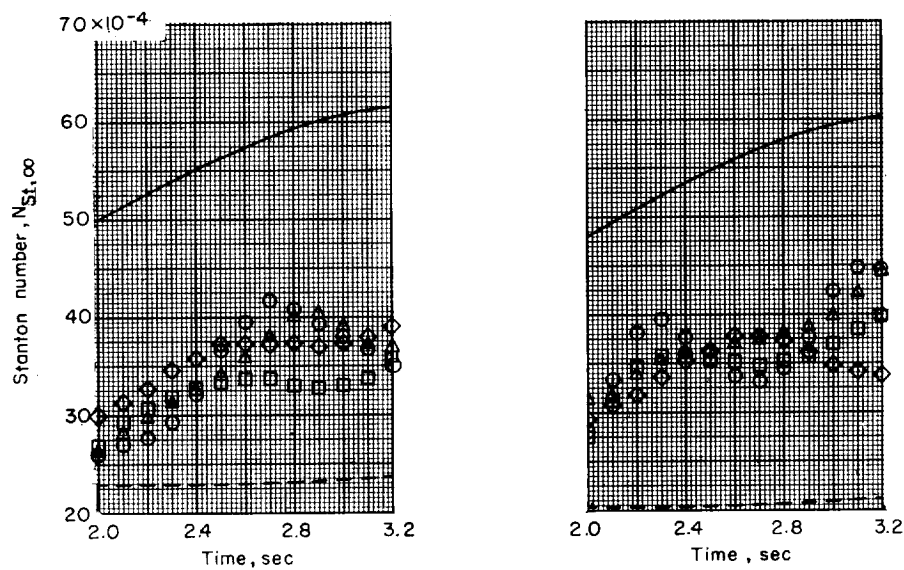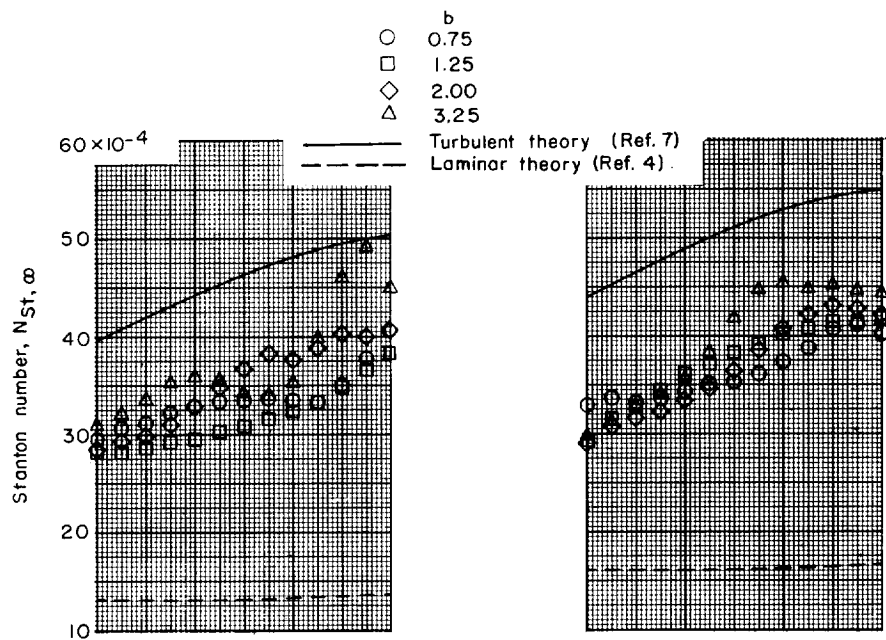
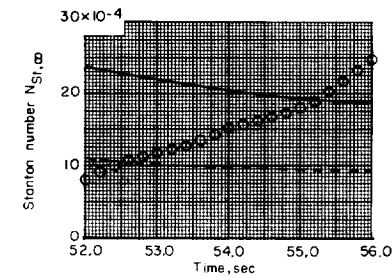Figure 11.- Comparison of experimental and theoretical Stanton number for the stagnation line of leading-edge segments.

(e) $\Lambda = 45^{\circ}$; $D = \frac{3}{4}$ inch.
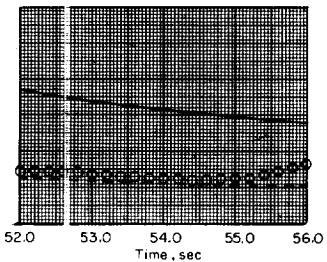
(f) $\Lambda = 45^{\circ}$; $D = \frac{1}{2}$ inch.

(g) $\Lambda = 45^{\circ}$; $D = \frac{1}{4}$ inch.

(h) $\Lambda = 36.75^{\circ}$; $D = \frac{1}{2}$ inch.
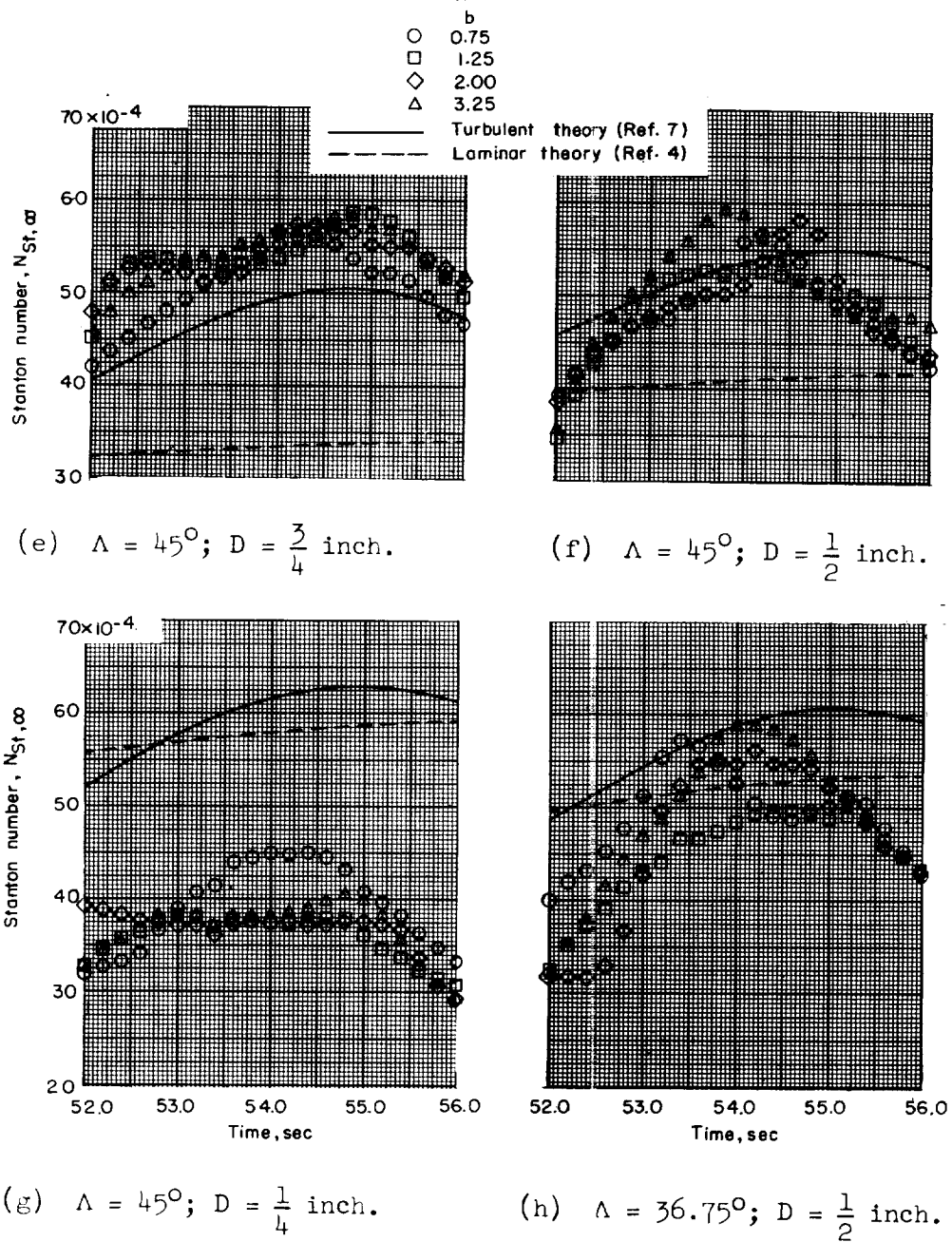
Figure 11.- Concluded.
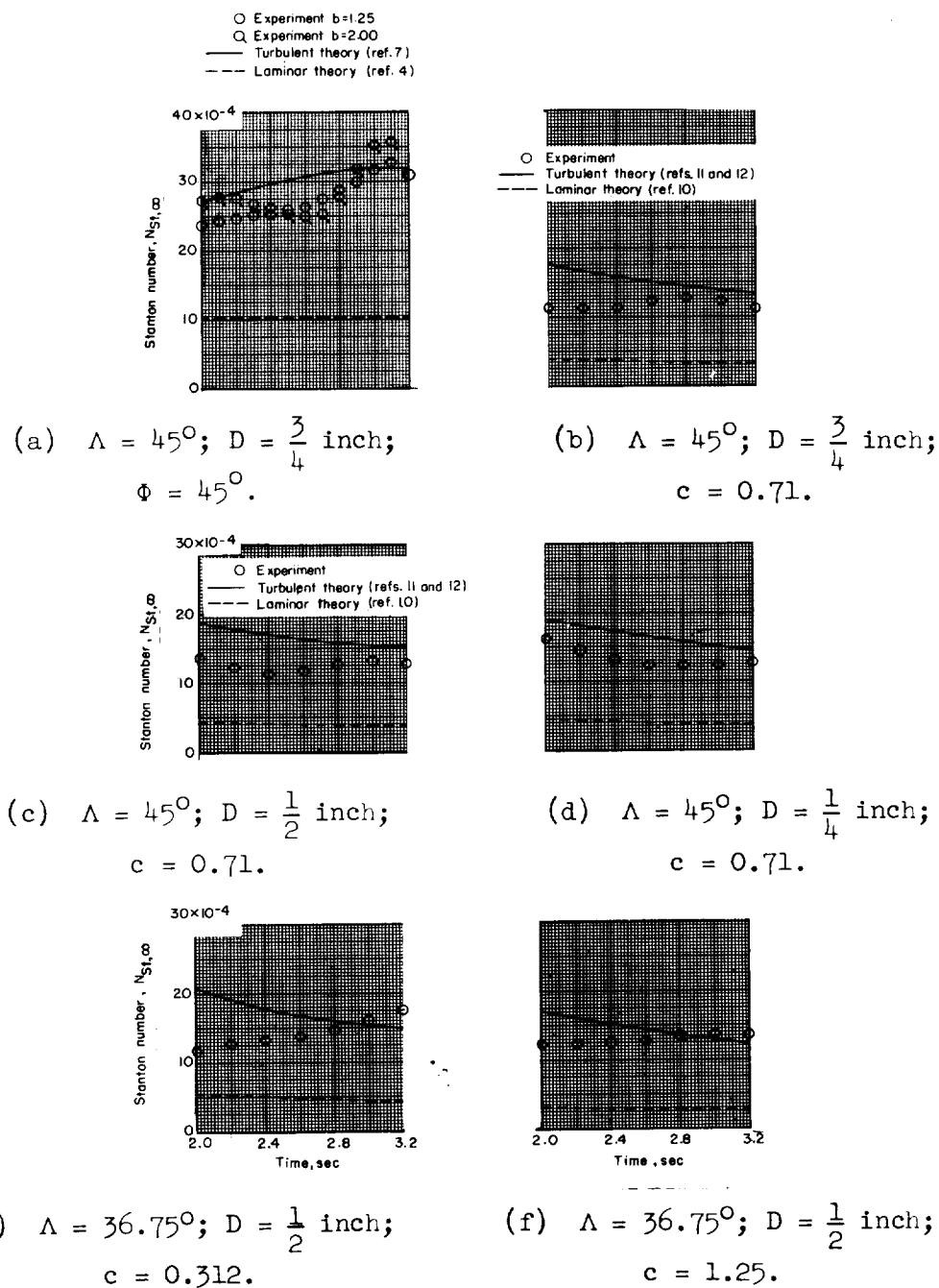
Figure 12.-Comparison of experimental and theoretical Stanton numbers back of stagnation line.
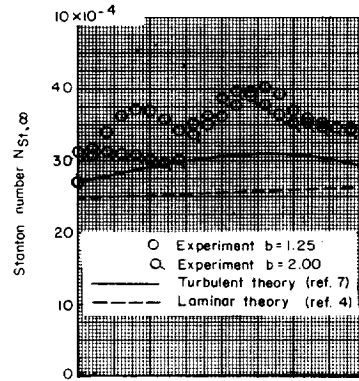
(g) $\Lambda = 45^\circ$; $D = \frac{3}{4}$ inch;

$\Phi = 45^\circ$.
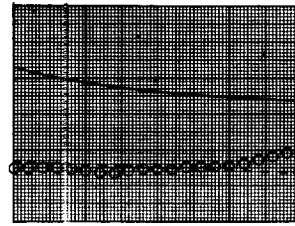
(h) $\Lambda = 45^\circ$; $D = \frac{3}{4}$ inch;
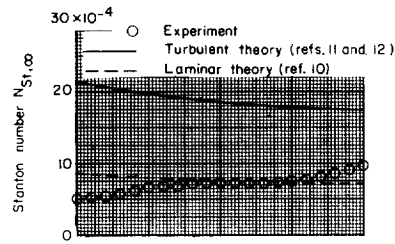
c = 0.71.

(i) $\Lambda = 45^\circ$; $D = \frac{1}{2}$ inch;

c = 0.71.
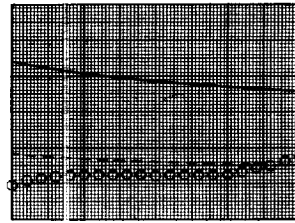
(j) $\Lambda = 45^\circ$; $D = \frac{1}{4}$ inch;

c = 0.71.

(k) $\Lambda = 36.75^\circ$; $D = \frac{1}{2}$ inch;

c = 0.312.

(l) $\Lambda = 36.75^\circ$; $D = \frac{1}{2}$ inch;
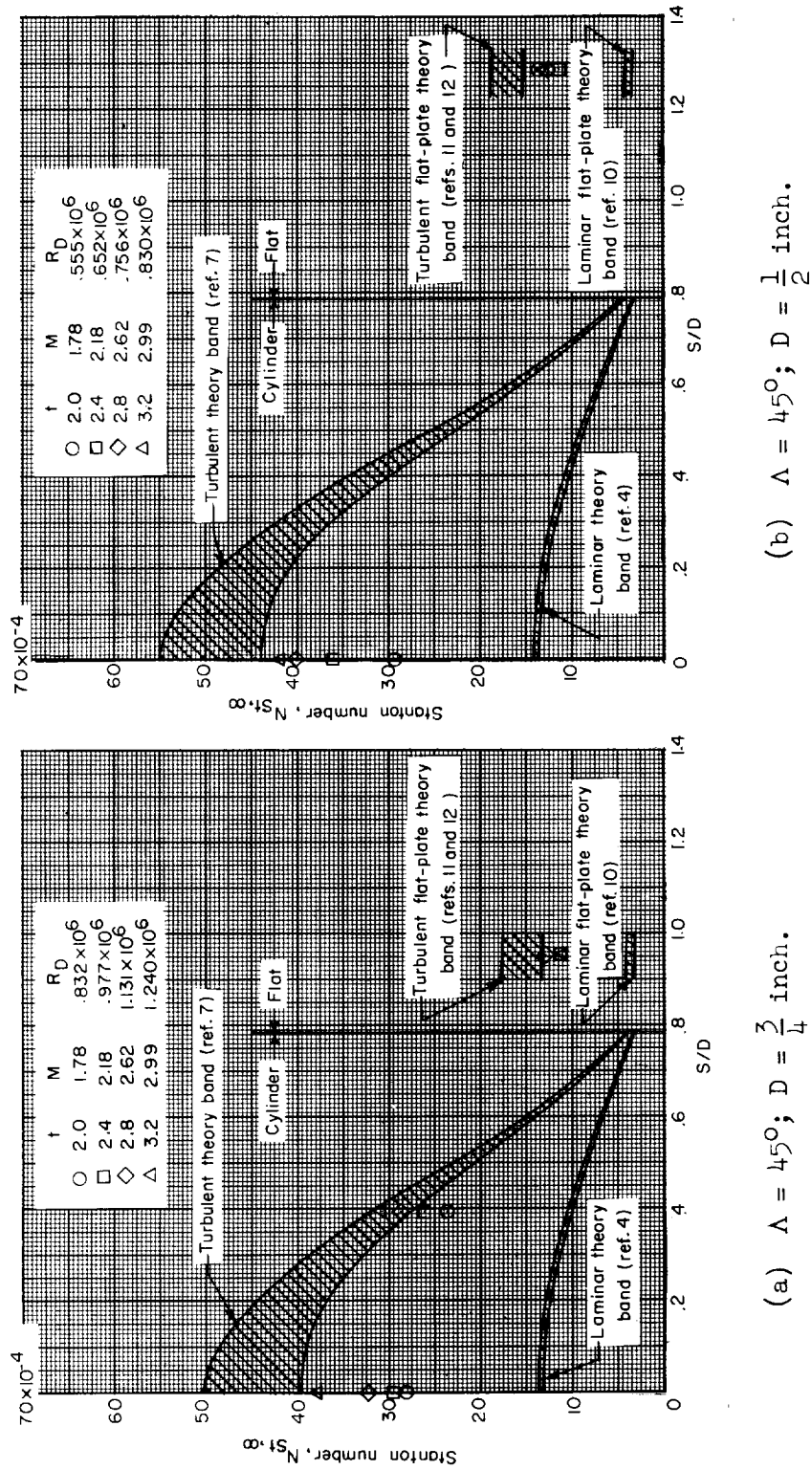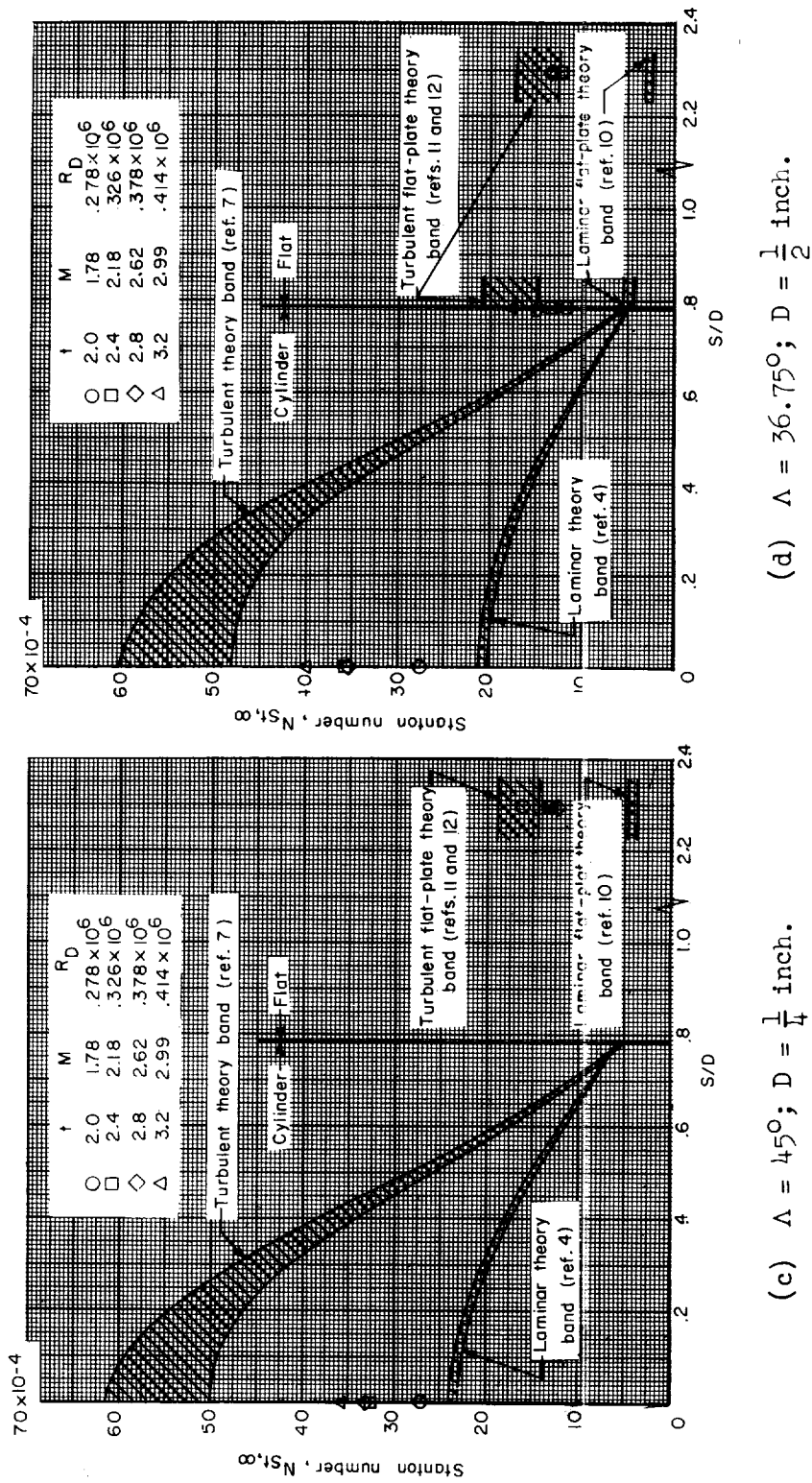
c = 1.25.

Figure 12.- Concluded.

(a) $\Lambda = 45°$; $D = \frac{3}{4}$ inch.

(b) $\Lambda = 45°$; $D = \frac{1}{2}$ inch.

Figure 13.- Chordwise distribution of experimental and theoretical Stanton numbers.
$b = 1.25$ inch.

(c) $\Lambda = 45°; \; D = \frac{1}{4}$ inch.
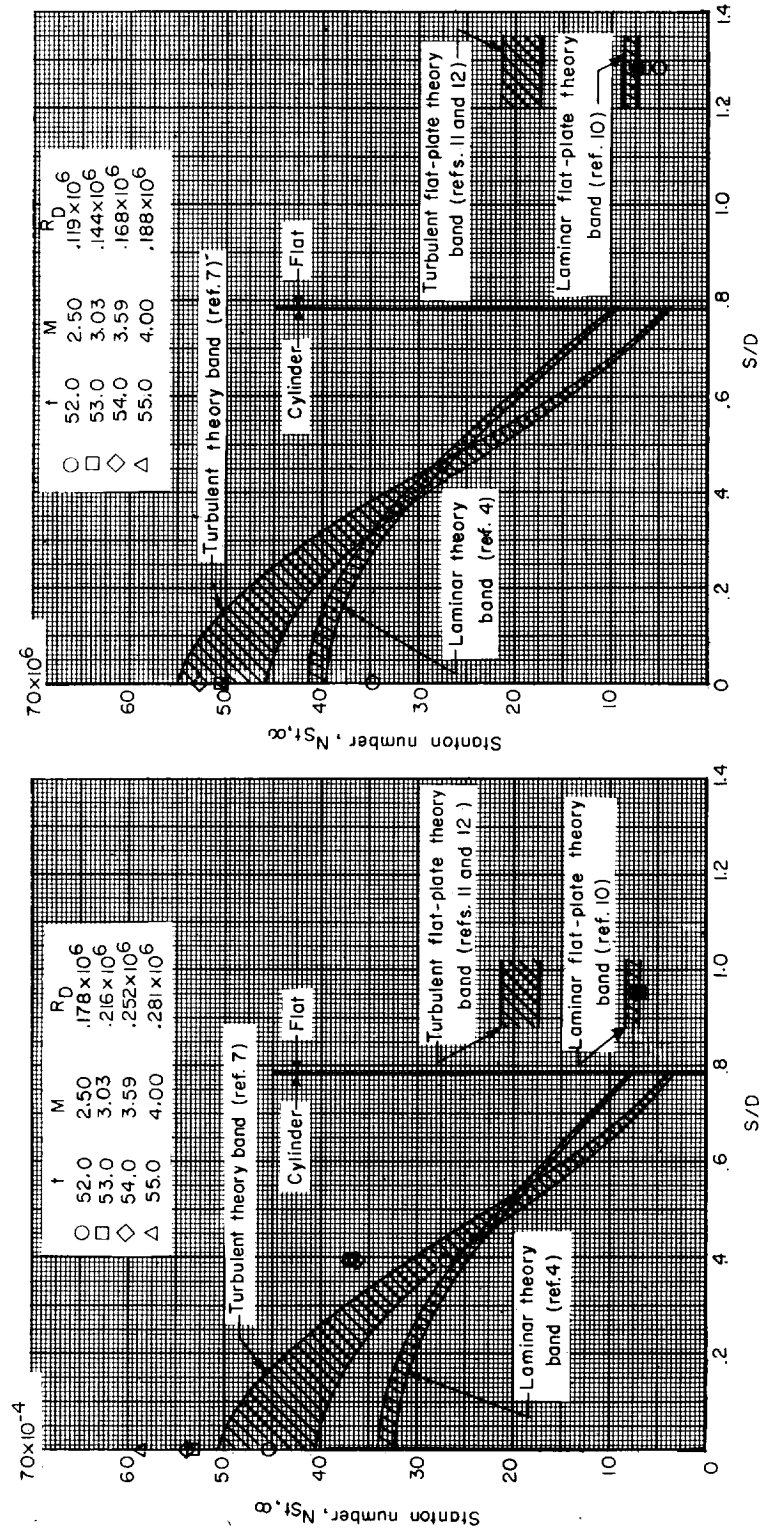
(d) $\Lambda = 36.75°; \; D = \frac{1}{2}$ inch.

Figure 13.- Continued.

(e) $\Lambda = 45°$; $D = \frac{3}{4}$ inch.

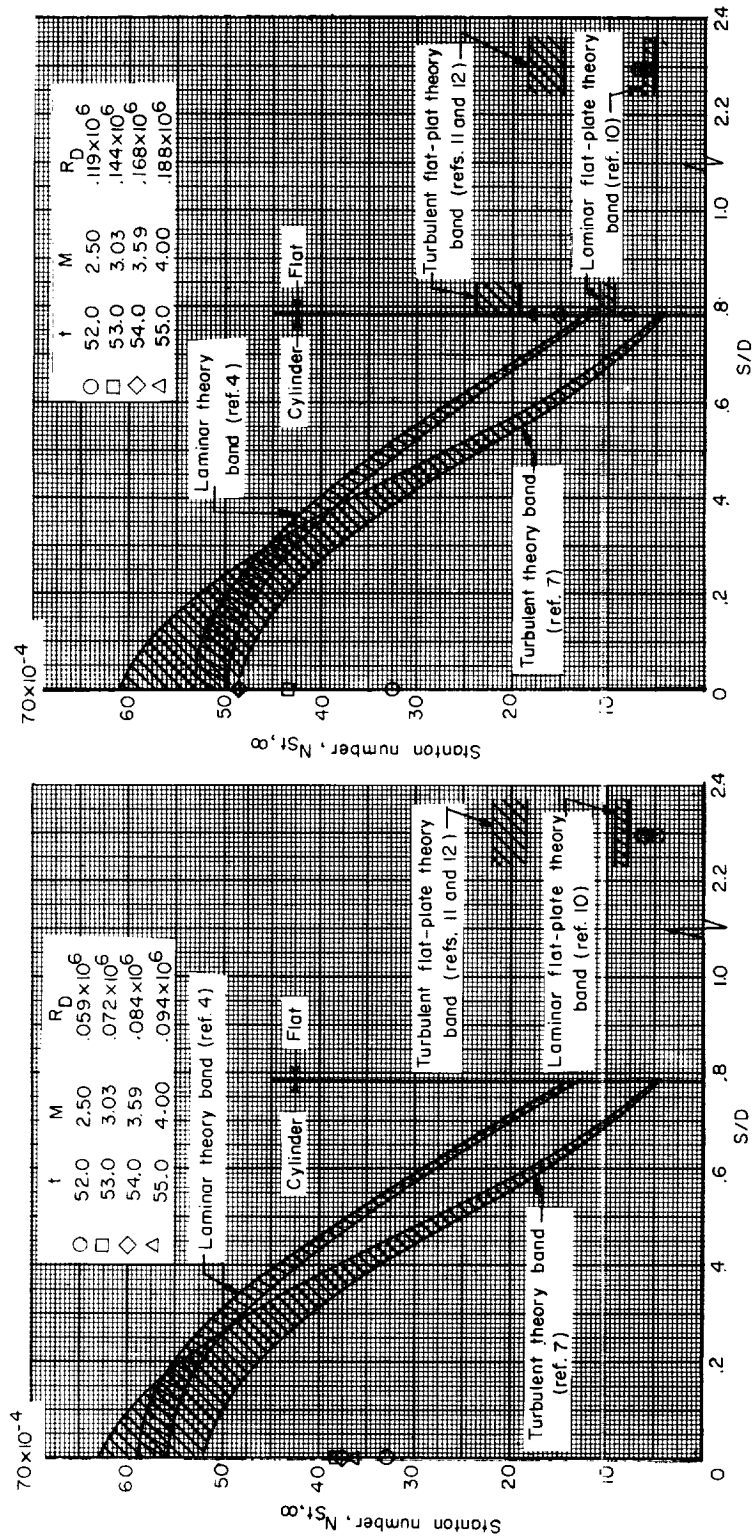(f) $\Lambda = 45°$; $D = \frac{1}{2}$ inch.

Figure 13.- Continued.

(g) $\Lambda = 45^\circ$; $D = \frac{1}{4}$ inch.

(h) $\Lambda = 36.75^\circ$; $D = \frac{1}{2}$ inch.
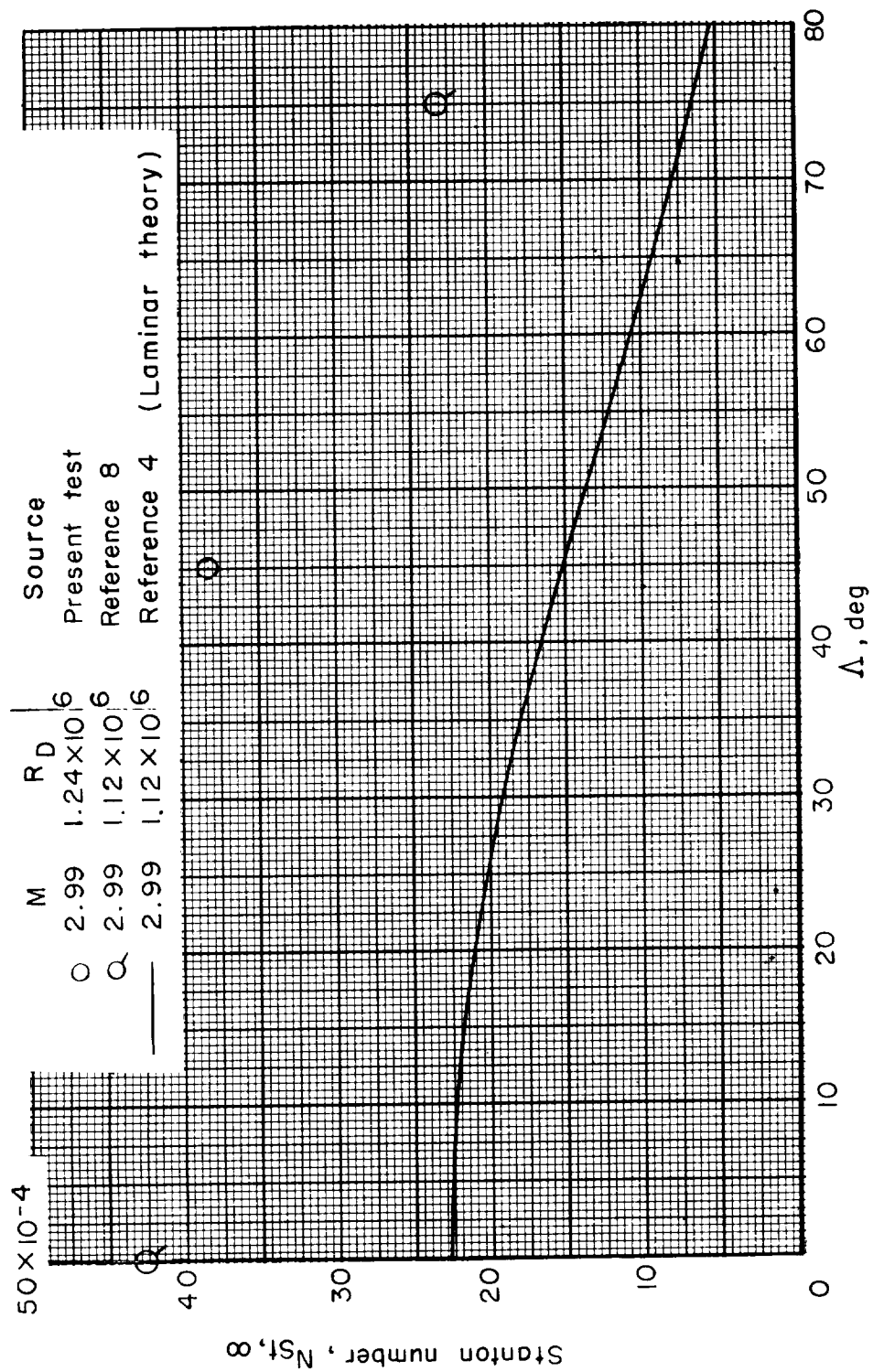
Figure 13.- Concluded.

Figure 14.- Effect of sweep on stagnation-line heat transfer. $D = \frac{3}{4}$ inch.